

Star-to-Star Abundance Variations among Bright Giants in the Mildly Metal-Poor Globular Cluster M4

Inese I. Ivans¹, Christopher Sneden¹, Robert P. Kraft², Nicholas B. Suntzeff³, Verne V. Smith^{4,5},
G. Edward Langer^{6,7}, Jon P. Fulbright²

Submitted to *The Astronomical Journal*

ABSTRACT

We present a chemical composition analysis of 36 giants in the nearby mildly metal-poor ($\langle[\text{Fe}/\text{H}]\rangle = -1.18$) “CN-bimodal” globular cluster M4. The stars were observed at the Lick & McDonald Observatories using high resolution échelle spectrographs and at CTIO using the multi-object spectrometer. Confronted with a cluster having interstellar extinction that is large and variable across the cluster face, we combined traditional spectroscopic abundance methods with modifications to the line-depth ratio technique pioneered by Gray (1994) to determine the atmospheric parameters of our stars. We derive a total-to-selective extinction ratio of 3.4 ± 0.4 and an average $\langle E(B-V) \rangle$ reddening of 0.33 ± 0.01 which is significantly lower than that estimated by using the dust maps made by Schlegel *et al.* (1998).

We determine abundance ratios typical of halo field and cluster stars for scandium, titanium, vanadium, nickel, and europium with star-to-star variations in these elements of $< \pm 0.1$. Silicon, aluminum, barium, and lanthanum are overabundant with respect to what is seen in other globular clusters of similar metallicity. These overabundances

¹Department of Astronomy and McDonald Observatory, University of Texas, Austin, TX 78712; iivans@astro.as.utexas.edu, chris@verdi.as.utexas.edu

²UCO/Lick Observatory, Board of Studies in Astronomy and Astrophysics, University of California, Santa Cruz, CA 95064; kraft@ucolick.org

³Cerro Tololo Inter-American Observatory, National Optical Astronomy Observatories, which is operated by the Association of Universities for Research in Astronomy, Inc., (AURA), under cooperative agreement with the National Science Foundation. La Serena, Chile; nsuntzeff@noao.edu

⁴Department of Physics, University of Texas at El Paso, 500 West University, El Paso, TX 79968-0515; verne@balmer.physics.utep.edu

⁵Visiting Astronomer, Cerro Tololo Inter-American Observatory, National Optical Astronomy Observatories, which is operated by the Association of Universities for Research in Astronomy, Inc., (AURA), under cooperative agreement with the National Science Foundation.

⁶Physics Department, Colorado College, Colorado Springs, CO 80903; elanger@academic.cc.colorado.edu

⁷Deceased 1999 February 16.

confirm the results of an earlier study based on a much smaller sample of M4 giants (Brown & Wallerstein 1992).

Superimposed on the primordial abundance distribution is evidence for the existence of proton-capture synthesis of carbon, oxygen, neon, and magnesium. We recover some of the C, N, O, Na, Mg, and Al abundance swings and correlations found in other more metal-poor globular clusters but the range of variation is muted. In the case of Mg and Al, this is compatible with the idea that the Al enhancements are derived from the destruction of $^{25,26}\text{Mg}$, not ^{24}Mg . We determine that the C+N+O abundance sum is constant to within the observational errors, and agrees with the C+N+O total that might be expected for M4 stars at birth.

The AGB stars in M4 have C,N,O abundances that show less evidence for proton-capture nucleosynthesis than is found in the less-evolved stars of the RGB. Deeply-mixed stars of the RGB, subsequent to the helium core flash, might take up residence on the blue end of the HB, and thus fail to evolve back to the AGB but reasons for skepticism concerning this scenario are noted.

Subject headings: globular clusters: individual (NGC 6121) — globular clusters: general — stars: abundances — nucleosynthesis — stars: fundamental parameters — dust, extinction

1. Introduction

Very large star-to-star abundance variations in the light elements C, N, O, Na, Mg and Al occur among the bright giants of a number of globular clusters. In clusters where giant star samples have been sufficiently large, the abundances of O and Na are anticorrelated, as are those of Mg and Al. Prime examples are found in M13 (Pilachowski *et al.* 1996; Shetrone 1996a,b, Kraft *et al.* 1997), ω Cen (Paltoglou & Norris 1989; Norris & Da Costa 1995a,b), NGC 6752 (Cottrell & Da Costa 1981), M15 (Snedden *et al.* 1997), and most recently NGC 3201 (Gonzalez & Wallerstein 1998). Recent major reviews of cluster abundance trends have been published by Suntzeff (1993), Briley *et al.* (1994), Kraft (1994), and Wallerstein *et al.* (1997).

Most investigators agree that the abundance anticorrelations arise from proton-capture chains that convert C and O into N, Ne into Na, and Mg into Al in the hydrogen-burning layers of evolved cluster stars. Controversy has arisen, however, between proponents of what are termed “evolutionary” *vs.* “primordial” scenarios. For a brief review of these alternatives, we refer the reader to the introductory section of Sneden *et al.* (1997). In the former picture one supposes that, in the low-mass red giants we presently observe, the products of internal proton-capture synthesis are brought to the surface by deep-mixing of the stellar envelope through the hydrogen-burning shell. Therefore, the anomalous behavior is expected to increase (on average) with advancing evolutionary state. In the latter scenario, one supposes that the proton-capture synthesis took

place in a prior generation of more massive stars. As a result of mass loss, these massive stars produced the required abundance redistribution in the primordial material out of which the presently observed low-mass stars were formed. Several lines of observational evidence now suggest that both scenarios may play important roles: superimposed on a primordial spread are additional variations resulting from deep-mixing in the stars we presently observe (*e.g.* Briley *et al.* 1994).

Stellar evolution theory (Sweigart & Mengel 1979) predicts that deep-mixing should become less efficient and possibly cut off as metallicity increases. Observational support for this hypothesis was found by Sneden *et al.* (1994), who showed that the C, N, O and Na abundances have little variation among giants in M71 ($[\text{Fe}/\text{H}] = -0.8$),⁸ whereas Sneden *et al.* (1992) did find variations in these elements in M5 ($[\text{Fe}/\text{H}] = -1.2$) similar to those in more metal-poor clusters such as M13, M15, and NGC 3201. However, the prediction fails to explain the differences between the CNO abundances of NGC 288 and NGC 362 (Dickens *et al.* 1991): these two clusters have very similar metallicities ($[\text{Fe}/\text{H}] = -1.40$ and -1.27 , respectively; Zinn & West 1984), yet one shows evidence for deep-mixing (redistribution of C, N and O abundances) whereas the other exhibits little or no variation in these elements. However, a new study by Shetrone (1999) indicates that both clusters, in fact, show wide variations among the C, N, and O elements, and that the earlier conclusions in declaring no variations in NCG 288 resulted from a limited sample size.

Variations in the cyanogen band strengths have also been studied extensively in the giant stars of old globular clusters, as well as nearby dwarf spheroidal galaxies. CN variations have been found in NGC 362, M5, M10, NGC 6352, NGC 7006, M92, M15, M71, M22, ω Cen, NGC 3201, NGC 6752, 47 Tuc and M4 (see *eg.* Smith & Norris 1982 and references therein) as well as in the Sculptor (Smith & Dopita 1983) and Draco (Smith 1984) dwarf galaxies. In clusters where a range in CN strengths is observed, there appears to be a correlation with elements such as oxygen, sodium, and aluminum. Examples include 47 Tuc and NGC 6752 (Cottrell & Da Costa 1981) and M22 (Smith & Wirth 1991), clusters spanning a metallicity range that encompasses M4. And, in some of the systems (NGC 6752, M22, ω Cen, and the dwarf galaxies), variations in calcium positively correlate with variations in cyanogen band strengths. Norris & Bessell (1978) were among the first to recognize the resemblance in chemical signatures between giants in M22, ω Cen, and the Sculptor and Ursa Minor dwarf galaxies. Extensive abundance studies of the three most interesting globular cluster systems of this kind have been done by Norris *et al.* (1981, NGC 6752), Twarog *et al.* (1995, M22) and Norris *et al.* (1996, ω Cen).

Given the importance of decoupling the evolutionary effects from primordial enrichments, these puzzles led us to consider an abundance study of a large sample of bright giants in the mildly metal-poor globular cluster M4. M4 (NGC 6121) is possibly the nearest globular cluster ($d \sim 1.7\text{--}2.1$ kpc; see Dixon & Longmore 1993 for a review). Despite the fact that M4 lies behind the outer portion of the Scorpius-Ophiucus dust cloud complex and thus suffers relatively high

⁸We adopt the usual spectroscopic notations that $[A/B] \equiv \log_{10}(N_A/N_B)_{\text{star}} - \log_{10}(N_A/N_B)_{\odot}$, and that $\log \epsilon(A) \equiv \log_{10}(N_A/N_H) + 12.0$, for elements A and B. Also, metallicity is defined as the stellar $[\text{Fe}/\text{H}]$ value.

reddening and extinction, its most luminous giants have relatively small apparent magnitudes and are readily accessible to detailed analysis. M4’s metallicity on the Zinn & West (1984) scale is $[\text{Fe}/\text{H}] = -1.3$. High-resolution spectroscopic estimates range from $[\text{Fe}/\text{H}] = -1.3$ (Brown *et al.* 1990; Gratton *et al.* 1986) through -1.2 (Brown & Wallerstein 1992) to -1.05 (Drake *et al.* 1992). Liu & Janes (1990) discuss M4 reddening and metallicity issues at length, and Drake *et al.* (1994) provide a useful summary table of the many metallicity estimates for this cluster. They compute a mean M4 metallicity, excluding their own result, of $\langle [\text{Fe}/\text{H}] \rangle = -1.17$. This metallicity is therefore near the anticipated cutoff in the deep-mixing process that leads to large light element abundance variations in red giant branch (RGB) stars of other clusters.

Norris (1981) discovered CN bimodality in M4: stars of similar luminosity exhibit a largely bimodal distribution of cyanogen strengths. Norris suggested that the distribution of CN band strengths among cluster giants could be related to the color distribution of stars on the horizontal branch (HB), *i.e.*, the so-called “second parameter” problem (*e.g.* Smith & Norris 1993). It is not clear, however, whether CN bimodality results from deep-mixing (variations in C \rightarrow N conversion among giants) or reflects instead some built-in primordial difference among cluster stars. Norris argued for a range in core rotational velocities inducing variable amounts of envelope mixing among the former main sequence stars that we now see as the M4 giants.

Previous abundance studies of the brighter giants in M4 present a rather complex picture. Brown & Wallerstein (1989) showed that C was depleted and N enhanced in four stars. They and Smith & Suntzeff (1989) found that M4 giants all had very low carbon isotope ratios, nearly the equilibrium ratio of $^{12}\text{C}/^{13}\text{C} \simeq 3.5$. This value is much lower than the ratio of 20 to 30 expected from the “first dredge-up” mixing episodes of Pop I giants (Iben 1964), and suggests the existence of a mixing mechanism more efficient than classical convection. Additionally, the Drake *et al.* (1992, 1994) analysis of two pairs of CN-strong and CN-weak giants found that the CN-weak pair had “normal” low abundances of Na and Al (*i.e.*, normal in comparison to field halo giants of comparable metallicity), whereas the CN-strong pair had significantly enhanced abundances of Na and Al. The CN-strong pair also had slightly (~ 0.2 dex) lower $[\text{O}/\text{Fe}]$ ratios than the CN-weak pair. These results are compatible with the deep-mixing hypothesis described above (Langer *et al.* 1993, Langer & Hoffman 1995, Langer *et al.* 1997).

On the other hand, Brown *et al.* (1990) found that M4 RGB stars have a relatively small (possibly insignificant) range of oxygen abundances compared with other clusters. Thus if deep-mixing is responsible for the changes in ^{12}C , ^{13}C and N, it may be that the mixing is not deep enough to penetrate those layers of the hydrogen-burning shell in which significant burning of O \rightarrow N takes place. Similarly, Brown & Wallerstein (1992) noted that their sample of M4 giants all had significant overabundances of Na (see also Gratton *et al.* 1986 and Gratton 1987) and Al, but not the corresponding depletions of O and Mg that might be expected if mixing had been deep enough to bring up the products of ON, NeNa and MgAl cycling.

To summarize, M4 RGB stars have been subjected to high resolution spectral analysis in

three independent investigations: Brown & Wallerstein (1992 and references therein; seven stars); Drake *et al.* (1992, 1994; four stars); and Gratton *et al.* (1986; three stars). However, there is little agreement among these investigations about the behavior of light element abundances. Unfortunately, the only overlap among these samples is M4 L3624 (Wallerstein, Leep, & Oke 1987; Drake *et al.* 1992, 1994). Moreover, the data sets and analysis techniques vary substantially among the investigations, so possible systematic effects in the abundances cannot easily be explored. The total sample size for M4 remains small.

We therefore have used the échelle spectrographs of McDonald and Lick Observatories to gather high resolution, large wavelength coverage, high signal-to-noise spectra of 25 M4 giant stars. Our spectrum analysis methodology yields values of T_{eff} independent of the photometric colors. This provides an independent measure of the reddening to each program star as well as the total-to-selective extinction ratio in the part of the dark cloud that obscures the cluster, a quantity believed to be anomalous (*e.g.* the review by Dixon & Longmore 1993). We have derived N and O abundances and $^{12}\text{C}/^{13}\text{C}$ ratios, abundances of the light elements Na, Mg, Al, Si, Ca, and Ti, the Fe-peak elements Sc, V, Fe and Ni, and the neutron-capture elements Ba and Eu. Additionally, we have used a multi-object spectrometer at the Cerro Tololo Interamerican Observatory to obtain medium-resolution spectra of 24 M4 giants. Thirteen of the stars in the medium resolution survey are also part of our high resolution sample, and the other eleven are generally giants of lower luminosity. These spectra have limited wavelength coverage, centered near $\lambda 6300 \text{ \AA}$, from which we derived [O/Fe] ratios. With this large sample of M4 giants we explore the distribution of several key light and heavy element abundances in M4.

2. Observations, Reductions, and Equivalent Width Measurements

M4 is possibly the nearest globular cluster ($d \sim 1.7\text{--}2.1$ kpc; see Dixon & Longmore 1993 for a review). Its giants are unusually bright; the RGB tip reaches $V \sim 10.5$. The cluster lies projected on rich star fields somewhat toward the Galactic nuclear bulge. Fortunately, proper motion (Cudworth & Rees 1990) and radial velocity (Peterson *et al.* 1995) studies have made selection of true M4 members fairly easy for stars as faint as two magnitudes below the HB. Assuming that M4 giants were only those with Cudworth & Rees membership probabilities $\geq 99\%$, we acquired high and medium resolution spectra for all 21 RGB stars with $V < 12.0$, and a total of 36 out of the 76 stars with $V < 13.1$.

The program stars are listed in Table 1; Lee (1977) identification numbers are used here and throughout this paper, with the exception of M4 G273, unobserved by Lee. Alternate star names with just a letter or a prefix A are those of Alcaino (1975), names with a prefix V are those of Sawyer Hogg (1973), and names with a prefix G are those of Greenstein (1939). The V and $B - V$ values are taken from the photographic photometry of Cudworth & Rees (1990). In Figure 1 we reproduce the total Cudworth & Rees M4 c-m diagram down to a V magnitude of 15.4 and show an enlargement of the region with $V < 13.1$. This figure demonstrates the evolutionary domain of

our program stars; the points in the enlargement are coded by the observatory and spectrograph resolution used to obtain each spectrum.

2.1. High Resolution Spectra

We gathered the high resolution spectra in 1997 using two échelle spectrographs equipped with large-format CCD detector systems: the McDonald Observatory 2.7m “2d-coudé” (Tull *et al.* 1995), and the Lick Observatory 3.0m “Hamilton” (Vogt 1987, Valenti *et al.* 1995). A standard set of tungsten filament lamp, Th-Ar hollow cathode lamp, “bias” and “dark” integrations accompanied the program star spectra. We also obtained spectra of several hot, rapidly rotating (essentially featureless) stars of similar airmass to M4. The effective wavelength range in both sets of spectra was $5200 \text{ \AA} \leq \lambda \leq 8800 \text{ \AA}$. The resolving power $R \equiv \lambda/\Delta\lambda$, as measured from the Th-Ar spectra, was $\simeq 60,000$ for most of the 2d-coudé data and $\simeq 50,000$ for the Hamilton data. A few fainter M4 giants were observed with the 2d-coudé at lower spectral resolving power ($R \simeq 30,000$). The lunar cycle was a concern; in order to minimize the amount of scattered moonlight in our spectra we avoided dates when the moon would be especially bright and close to M4 in the sky. Table 1 lists dates and places of the observations, total exposure times (which sometimes represent the sum of two or three individual integrations), as well as the estimated signal-to-noise ratios in the final co-added reduced spectra near $\lambda 6350 \text{ \AA}$; for the whole sample, $\langle S/N \rangle \simeq 80$.

Initial spectrum reductions included correction for the CCD frame bias level, trimming of the frame overscan region, division by flat field frames, interpolation over bad pixels and anomalous radiation events, removal of scattered light underlying the spectral orders, extraction of the individual orders, and implantation of a wavelength scale with the aid of the Th-Ar integrations. These we accomplished using standard routines in IRAF⁹ and, for the Hamilton data, VISTA (Goodrich & Veilleux 1988) software packages; see previous papers in this series (*e.g.*, Sneden *et al.* 1991, Kraft *et al.* 1993) for further discussion of these procedures.

The resulting singly-dimensioned spectra were processed further with specialized software (SPECTRE: Fitzpatrick & Sneden 1987) in order to compute radial velocities, continuum-normalize the spectra, remove telluric spectral features, and measure equivalent widths. During these tasks it became apparent that star L1412 could not be treated in the same manner as the other program stars. Our spectra reveal much broader absorption lines in L1412 than in any other M4 giant and one that varied significantly over a one-year period, not only in radial velocity but in line depth ratios of temperature-sensitive lines. At $V = 10.38$, this star is by far the brightest M4 cluster member, and the aberrant nature of its spectrum (particularly the very strong CN and detectable TiO bands) has been well documented in the literature. Whitmer *et al.* (1995, and

⁹IRAF is distributed by the National Optical Astronomy Observatories, which are operated by the Association of Universities for Research in Astronomy, Inc., under cooperative agreement with the National Science Foundation.

references therein) have recently discussed L1412 in some detail, concluding that it is a post-AGB star. This star would have required a very different analysis than that employed for the rest of our sample, and so we dropped it from further consideration in this study.

We used the stellar radial velocities v_r to recheck cluster membership for our program stars and to compare with velocity estimates in the literature.¹⁰ The v_r values were computed by comparing the measured line-center wavelengths of 13 lines in the $\lambda 6300 \text{ \AA}$ order to those listed in the catalogue of solar lines by Moore *et al.* (1966) and converting to velocity units. Similar measurements of telluric O_2 line wavelengths on the same échelle order set the zero point of the velocity scale for each spectrum. Each line center was determined by eye to about $1/3$ pixel ($\sim 2 \text{ km s}^{-1}$) accuracy. For stars that were observed twice in one night, our mean v_r determinations agree very well, with a scatter of 0.1 km s^{-1} . The mean v_r and the standard deviation for each star are entered in Table 1, along with the values of Peterson *et al.* (1995). The agreement with their work is excellent: taking the differences in the sense *this study minus Peterson et al.*, $\langle \delta v_r \rangle = -0.18 \pm 0.23 \text{ km s}^{-1}$ ($\sigma = 0.99 \text{ km s}^{-1}$, for 21 stars in common).

M4, with a declination of -26.5° , never rises higher than an altitude of $\simeq 32^\circ$ at McDonald Observatory and $\simeq 25^\circ$ at Lick Observatory. Telluric O_2 and H_2O spectral lines often are very strong at such large airmasses, and special care must be taken in the cancelation of these features via division by the “telluric standard” hot-star spectra. With a careful choice of divisor star (very early spectral type, large *vsini*, and best airmass match to M4), and through modest manipulation of the divisor telluric line strengths in SPECTRE, we achieved essentially complete removal of telluric features. We illustrate this by one example shown in Figure 2. But, even with such a robust procedure, residual telluric feature contamination might be of concern for the analysis of the important $\lambda 6300.3 \text{ \AA}$ [O I] line. Fortunately, the average cluster radial velocity of $\sim +70 \text{ km s}^{-1}$ translates to a red shift of more than 1 \AA , leaving the stellar [O I] well clear of any O_2 absorption line, as well as the night sky [O I] emission line.

Even though M4 has a metallicity of less than one-tenth solar, its upper RGB stars have strong and complex spectra; special care must be taken in continuum placement. For each spectral order the continuum was set by interactively fitting a spline function to line-free spectral regions. Locating the continuum was aided by comparing the spectra of our program stars with that of Arcturus (Griffin 1968).

We initially adopted the atomic line lists used in previous papers of this series, but after careful line-by-line inspection of both our spectra and that of the Arcturus atlas, we culled

¹⁰Our preliminary reconnaissance of the spectrum of M4 L4513, suggested to be a 99% probable member from the star’s proper motion (Cudworth & Rees 1990), revealed a discordant radial velocity (more than 110 km s^{-1} blueshifted with respect to the cluster mean velocity). Peterson *et al.* (1995) also noted this star’s discrepant velocity, rejecting it as a cluster member. Additionally, the T_{eff} we derived for this star (with an identical analysis to the other M4 targets) produced implied colors and absolute magnitudes very different than those of the rest of our sample. We therefore discarded L4513 from this study.

four lines which seem to be too blended to be used in cool RGB stars having M4’s metallicity. Unfortunately we were then left with a list of only fairly strong lines, and so we added as many clean lines of low–medium strength as were available from Langer *et al.* (1998), Lambert *et al.* (1996), and Thévenin (1990). We also included in our line lists the La II lines of Brown & Wallerstein (1992) and these line choices will be discussed further in §3.5. We measured equivalent widths (EWs) for these lines with SPECTRE, using Gaussian approximations for all but the strongest lines, for which Voigt profile fits were employed. The tables of EWs and associated atomic parameters are too large to include here, but are available electronically from the first author. We did not analyze any line with $\log(\text{EW}/\lambda) > -4.25$ with the exception of those of Ba II. Such strong lines are too sensitive to choices in both microturbulent velocity and line damping constant to yield reliable abundances. We did retain lines of Ba II (which has only very strong transitions); those were treated with synthetic spectrum computations as described in §3.

Our EWs agree reasonably well with those in the literature. Taking comparisons in the sense *this work minus others*, for the four stars in common with Drake *et al.* (1992), $\langle \delta\text{EW} \rangle = +1.4 \pm 0.8 \text{ m}\text{\AA}$ ($\sigma = 5.2 \text{ m}\text{\AA}$, 43 lines). We also made independent measurements of some of the lines used in the Drake *et al.* study, as well as some of the additional lines used in the present study. Comparison with those measures revealed consistency with ours: $\langle \delta\text{EW} \rangle = +2.5 \pm 0.7 \text{ m}\text{\AA}$ ($\sigma = 4.4 \text{ m}\text{\AA}$, 45 lines). We have three stars in common with Brown *et al.* (1990) neglecting L1412, and Brown (1998) has kindly made available to us their unpublished EW measurements. Our EW scale has a small negative offset from theirs, and there is significant line-to-line scatter: $\langle \delta\text{EW} \rangle = -6.9 \pm 1.3 \text{ m}\text{\AA}$ ($\sigma = 10.9 \text{ m}\text{\AA}$, 66 lines). We suspect that the offset arises from the large difference in spectral resolving powers of the two studies: our spectra of these stars were obtained at $R \simeq 60,000$, while the Brown *et al.* spectra had $R \simeq 20,000$. There are CN lines throughout the red spectral region, and it is difficult to avoid inclusion of one of them in EW measurements. Our higher spectral resolution undoubtedly aided in spotting CN lines lurking in the wings of some atomic lines, hence our mean EWs would be expected to be lower.

2.2. Medium Resolution Spectra

In 1992 we surveyed M4’s RGB with the CTIO 4m Argus fiber-coupled multi-object spectrometer (Ingerson 1993). The spectra were obtained to study the strongest [O I] feature, and so were centered at $\lambda 6300 \text{ \AA}$. The spectral coverage was approximately $6240 < \lambda < 6360 \text{ \AA}$, the reciprocal dispersion was $\simeq 0.2 \text{ \AA}/\text{pixel}$, and the effective resolving power was $R \simeq 20,000$. We obtained spectra of 24 M4 giants and used the 24 remaining Argus fibers to gather sky spectra. As with the high resolution data, we acquired companion spectra of a flat-field lamp source, a hot rapidly-rotating star, and a Th-Ar emission line lamp. The flat-field lamps were projected onto the 4-m dome and observed through the telescope light path. We also observed the twilight sky with Argus to aid in the wavelength identifications.

The Argus frames were reduced to one-dimensional wavelength-calibrated spectra with

standard IRAF routines (see Suntzeff *et al.* 1993 for a detailed discussion of the reduction of the Argus fiber data). The data reduction included sky subtraction with mean spectra chosen from the 24 sky fibers. Argus has a substantial focus change going from fiber 1 to 48 along the entrance slit to the spectrograph (perpendicular to the dispersion), resulting in a detectable spectral resolution difference among the fibers. The sky spectra were formed from the seven sky fiber spectra nearest to the program fiber spectra. The M4 data were observed in three exposures. The reduced data were co-added and the final spectra represent a total integration time of 95 minutes.

Radial velocities were measured with respect to a single velocity template. All the fibers were put on a common relative system for a single CCD exposure, and then all of the frames during the night were put on the same relative system by cross-correlating all the Th-Ar spectra and applying a zero point to each frame. We then demanded that the average velocity of M4 be the same as the average velocity of the Peterson *et al.* (1995) stars observed in common, bringing our velocities onto their absolute velocity system. The observed dispersion about the (defined zero) mean was 0.8 km s^{-1} with respect to Peterson *et al.*

We used SPECTRE to carry out telluric line cancelation. The telluric standard hot-star spectra were obtained in multiple fibers. For each program star spectrum, we co-added (to increase S/N) the reduced telluric hot-star spectra from several of the nearest fibers surrounding the slit position of the program star fiber before applying the telluric cancelation routines.

In Figure 3 we show two fully reduced Argus medium-resolution spectra of stars for which we also obtained high resolution data. The stars chosen for display illustrate the appearance of the spectra (intrinsic line strengths and S/N of the data) for a star near the RGB tip and one near the low-luminosity limit of the high-resolution targets. The [O I] $\lambda 6300.3 \text{ \AA}$ line is marked, and we also draw attention to several V I and Ti I lines in this spectral region. Their large sensitivity to $B - V$ (hence T_{eff}) is apparent from these spectra. However, none of these lines are among those recommended by Gray (1994) for line-depth ratio studies (potential contamination by O₂ telluric lines limit their utility for ultra-precise T_{eff} measurements). The sacrifice of resolution in order to gain stellar sample size is easily seen in the Argus spectra of this figure. There are few if any truly unblended spectra features over the 120 \AA spectral range of these data. Therefore we measured no EWs on the Argus spectra and performed no line-by-line abundance analysis. However, the [O I] line is clearly detected in all Argus targets, and we were able to derive reliable [O/Fe] ratios from these data via synthetic spectrum analyses, after first analyzing the high resolution data and using those results to anchor the computations for the medium resolution spectra.

3. Abundance Analysis

In this section we describe the derivation of abundances in our samples of M4 giants. We consider two very different spectroscopic data sets for a cluster that presents unusual analytical difficulties irrespective of the data characteristics. Analysis of the high resolution data is discussed

in the first several subsections, and the last subsection is devoted to the medium resolution data.

3.1. The Special Challenges of M4 Giant Star Spectra

The translation of EWs from high resolution spectra into reliable abundances depends on the accurate determination of four stellar atmosphere parameters: effective temperature T_{eff} , gravitational acceleration $\log g$, overall metallicity $[\text{Fe}/\text{H}]$, and microturbulent velocity v_t . A distinct advantage of most globular cluster abundance analyses is the ability to use cluster c-m diagram photometry to specify preliminary values of T_{eff} and $\log g$, thereby leaving essentially only $[\text{Fe}/\text{H}]$ and v_t as free parameters to be determined from spectral line analysis. We have used this technique in many of our previous papers, but it cannot be done in M4 (nor can it be employed for many higher metallicity “disk population” globular clusters). The insurmountable difficulty here lies in the large and differential reddening across the face of M4 produced by the complex Sco-Oph dust distribution. Reddening cannot reliably be estimated for individual M4 stars to the level needed to map broad-band photometric indices onto stellar parameters. The spatial variability of reddening in M4 does not permit even a reliable photometric *ranking* of our stars in order of T_{eff} . Moreover, all bright M4 giants have strong-lined spectra, and that adds to the frustrations: cleanly measurable absorption lines usually lie on the flat (saturated) part of the curve-of-growth, so that plausible abundances may be obtained for a variety of assumed T_{eff} , $\log g$ and v_t combinations. A different strategy must be employed, and after conducting a number of numerical experiments we constrained M4 stellar effective temperatures with the following technique.

We first adopted a modified version of the method originally described by Gray & Johanson (1991) that uses the ratios of central depths of lines having very different functional dependences on T_{eff} to derive accurate relative temperature estimates. The T_{eff} calibration of the M4 line depth ratios was set through a similar analysis of RGB stars of M5 (a cluster of very similar metallicity to M4 but little reddening problem). Then, in order to anchor the T_{eff} scale and to lift most of the remaining stellar parameter degeneracies, we demanded that abundances determined from Ti I and V I lines yield $[\text{Ti}/\text{Fe}]$ and $[\text{V}/\text{Fe}]$ abundance ratios that (a) did not appreciably vary from star-to-star in M4, and (b) were roughly consistent with those ratios that have been derived in our previous studies of other, more easily analyzed globular clusters. Ti I and V I have much lower ionization potentials than does Fe I, and available spectral features of these two species arise from lower excitation states than do the typical Fe I lines we employed. Their derived relative abundances are thus very sensitive to T_{eff} . We further demanded that the $[\text{Fe}/\text{H}]$ abundance ratios fall within the range $-1.05 \geq [\text{Fe}/\text{H}] \geq -1.30$, as suggested by the earlier M4 analyses cited in §1. However, $[\text{Ni}/\text{Fe}]$ was left free to vary from any and all constraints. Finally, we estimated gravities by obtaining equality in abundances of neutral and ionized species of both Fe and Ti.

The “Gray” method is a purely *empirical* match between measured line depth ratios and photometric indices and/or T_{eff} scales; its use requires no defense here. More justification is

needed for our other assumptions in stellar model determinations. If the chief goal of this work is to search for star-to-star element abundance variations, how can we insist on little scatter in the relative Ti and V abundances? The arguments here are both theoretical and observational. First, V and Ni are part of the “Fe-peak”, and are synthesized together with Fe during the most advanced quiescent and explosive core fusion stages of high mass stars. Ti has a more complex nucleosynthetic origin, being produced both as an Fe-peak element and as the heaviest identifiable “ α -capture” element. In field metal-poor stars, at least over the metallicity range $-1.0 \geq [\text{Fe}/\text{H}] \geq -2.5$, observers agree that $[\text{V}/\text{Fe}] \simeq [\text{Ni}/\text{Fe}] \simeq 0.0$, while $[\text{Ti}/\text{Fe}] \simeq +0.3$ (*e.g.*, Gratton & Sneden 1991, and references therein). The star-to-star scatters in these means are very small, consistent with being dominated by observational errors. Corresponding cluster abundances are in complete accord with the field star values. From earlier papers in this series, straight means of the average abundance ratios in M3 and M10 (Kraft *et al.* 1995), M13 (Kraft *et al.* 1997), M5 (Sneden *et al.* 1992), M92 (Sneden *et al.* 1991), M15 (Sneden *et al.* 1997), and NGC 7006 (Kraft *et al.* 1998), are: $\langle [\text{Ti}/\text{Fe}] \rangle = +0.26$ ($\sigma = 0.04$; no value for M15 and M92); $\langle [\text{V}/\text{Fe}] \rangle = -0.01$ ($\sigma = 0.04$); and $\langle [\text{Ni}/\text{Fe}] \rangle = -0.01$ ($\sigma = 0.09$; no values for M15 and M92). We expect these values to approximately hold in M4.

3.2. Line Depth Ratios Applied to M4 Effective Temperatures

Gray & Johanson (1991) demonstrated that the ratio of the central depth of V I $\lambda 6251.83 \text{ \AA}$ to that of Fe I $\lambda 6252.57 \text{ \AA}$ is correlated very strongly with $B - V$ and T_{eff} in Pop I main sequence F7–K7 stars. Their work was developed by Gray (1994) to include more line pairs, and Hiltgen (1996) further extended the method to G–K subgiants over a larger range of disk metallicities. Happily, many of Gray’s line depth ratios are also sensitive T_{eff} indicators for lower metallicity very cool RGB stars. We illustrate this in Figure 4 with reproductions of spectra of two M4 stars that have $\delta T_{\text{eff}} \sim 700 \text{ K}$. In this temperature regime, the strengths of V I lines clearly increase with decreasing T_{eff} while Fe I lines change very little in M4 RGB stars. Other features employed by Gray change more slowly, but all ratios retain some sensitivity to T_{eff} .

In Figure 5 we show the correlations of two Gray ratios with temperature in three clusters previously studied in this series.¹¹ The illustrated ratios are d8/d7 (or V I $\lambda 6223.20 \text{ \AA}/\text{Fe I } \lambda 6229.23 \text{ \AA}$) and d5/d6 (or V I $\lambda 6224.51 \text{ \AA}/\text{Fe I } \lambda 6226.74 \text{ \AA}$). The T_{eff} values are taken from Sneden *et al.* (1992) for M5, Kraft *et al.* (1995) for M10, and Kraft *et al.* (1997) for M13. Data for M4 also are included in this figure, and they are developed in the present and next section. Figure 5 shows quantitatively how the (base-10 logarithm of) line depth ratios vary more than one dex in spectra of giants of moderately metal-poor clusters, and thus can indicate very small T_{eff} changes. These relationships begin to flatten out among the coolest stars, as both dividend V I and divisor

¹¹A comprehensive investigation of the spectroscopic line ratios of these data sets is underway and will be reported in a future publication.

Fe I line strengths begin saturating, and their central depth ratios approach unity. Thus these ratios probably will be less useful as temperature indicators for the coolest stars of appreciably more metal-rich globular clusters. Clusters with $[\text{Fe}/\text{H}] > -1$, such as 47 Tuc and M71, have redder (thus cooler) RGBs than M5 and M4, and the combination of lower T_{eff} and higher $[\text{Fe}/\text{H}]$ conspire to saturate and blend virtually all of the usual spectral features.

Turning the line depth ratios into temperatures requires some calibration steps, and here we describe the procedure used for M4. We first considered M5, a cluster whose metallicity ($[\text{Fe}/\text{H}] = -1.17$; Sneden *et al.* 1992) is similar to M4, but which suffers very little interstellar dust extinction ($E(B - V) = 0.03$, or $A_V \simeq 0.1$; Frogel *et al.* 1983). We measured all line depth ratios for M5 recommended by Gray (1994) that appear on the Hamilton spectra of 13 stars previously treated by Sneden *et al.* and 20 stars newly observed with the Keck “HIRES” échelle spectrograph.¹² We correlated the line depth ratios against de-reddened M5 $B - V$ values from Cudworth (1979) and Simoda & Tanikawa (1970), and fit linear or quadratic regression lines to these data to create formulae to predict $B - V$ ’s from the depth ratios.

We then measured the line depth ratios in our M4 stars and used the M5 formulae to predict a $(B - V)_o$ value for each ratio in each M4 star. Weighted means were then computed for each star, with the weights directly proportional to the slopes of the logarithmic depth ratio *vs.* $B - V$ regression relationships and inversely proportional to the observed scatters around these relationships. These implied colors were compared to the M5 temperatures derived by Sneden *et al.* (1992) to produce initial M4 T_{eff} estimates. Such T_{eff} ’s were expected to be accurate for *ranking* the stars; zero-point (or slope) offsets from M5 T_{eff} ’s remained to be determined from full spectral analyses.

3.3. Final Model Parameters

As discussed in §3.1, we used line-by-line abundance analyses to complete the model atmosphere specifications. We employed the current version of the LTE line analysis code MOOG (Sneden 1973) for these computations. As in earlier papers of this series, we input to MOOG trial model atmospheres generated with the MARCS code (Gustafsson *et al.* 1975) and the atomic line data described in §2. A few comments on the line lists should be made here. First, Ni and Fe have similar first ionization potentials and atomic structures. We expected the scatter in $[\text{Ni}/\text{Fe}]$ to provide additional information regarding how well the $[\text{Fe}/\text{H}]$ abundances had been determined. Therefore a special effort was made to identify as many clean Ni I lines as possible; we eventually used nine lines in most stars. Second, many V I transitions have large hyperfine splitting. Since these lines often are very strong in M4 giants, we limited our analysis to V I $\lambda\lambda 6274.6$ and 6285.1 \AA , two lines with well-determined laboratory hyperfine structure components (as reported

¹²A comprehensive analysis of these M5 data sets will also be reported in a future publication.

by McWilliam & Rich (1994)), normalizing the gf-values to those adopted for these lines in our previous work. We used the blended-line option of MOOG to derive abundances from the EWs of these lines. Finally, we added the $\lambda 6606.9 \text{ \AA}$ line of Ti II to our previously employed Ti I lines, in order to provide a second ionization equilibrium check.

Iterative abundance runs with small excursions in T_{eff} , $\log g$, model $[M/H]$, and v_t yielded the final model parameters; these are listed in Table 2. Recalling from §3.1 that there is much coupling among the model parameters and no assistance to be had from photometry, we concentrated on the following abundance indicators for the model iterations. For T_{eff} : no obvious trends of Fe I abundances with excitation potential; sensible Ti and V abundances ($[Ti/Fe] \sim +0.3$, $[V/Fe] \sim 0.0$); and Fe abundances within the range $-1.05 \geq [Fe/H] \geq -1.30$ (again, as suggested by several previous analyses). For $\log g$: consistent abundances from lines of neutral and ionized species of Fe and Ti; reasonable predicted c-m diagram positions with the derived gravities (see §3.4). For v_t : no obvious trends of Fe I line abundances with EWs. The whole set of iterated models was rechecked for consistency with the T_{eff} rankings derived from the initial line depth ratio calibrations. Overall, we demanded that the Ti, V, and Fe abundances show no significant drifts along the M4 RGB.

These model constraints appear to be so restrictive that they virtually guarantee particular sets of model parameters. But, in reality, the nearly 1000 K range in T_{eff} is quite helpful, for there is no astrophysical reason for the Fe-peak abundances to vary significantly from star to star along the M4 giant branch. The model parameter couplings are much less severe in the warmer stars of our high resolution sample, and those stars yield *without constraint* the abundance ratios suggested above. Note also that for all stars, the abundances deduced from Ti I and V I work together: the $[Ti/V]$ ratios are nearly insensitive to model parameter choices. Finally, inspection of Figure 5’s correlation between the line depth ratios and our final T_{eff} estimates for M4 giants suggests reasonable agreement. Our M4 T_{eff} scale is on the same general system as that employed in our earlier investigations of M5, M10, and M13.

In the three coolest M4 stars (L1514, L4613, and L4611) we were unable to satisfy all of the constraints equally well. The abundances for these stars, where they appear in the figures that follow, have been marked with a hollow square symbol (\square). The MARCS models we used for all stars assume LTE. For these cool stars at the tip of the giant branch, with their extended envelopes and extremely low $\log g$ values, formation of Fe I and other lines in the atmospheres may be affected by departures from LTE. If Fe and Ti are over-ionized in the outer layers of these very low density giants, the gravities we obtain by demanding ionization equilibrium will be too low. In the abundance results based on the fundamental parameters we adopted for these three stars, the ionization equilibrium between Ti I and Ti II and between Fe I and Fe II were not satisfied equally well. The abundances of V and Ti also indicate that the stellar models adopted for these cool stars may not be the most suitable. It is possible that we reached beyond the useful limits, in temperature and gravity, of the MARCS model atmospheres and/or the LTE line formation assumptions of the analysis code for these coolest stars.

We performed numerical experiments to determine systematic and random errors of our model parameters. Based on the “degeneracy” of the models to fit the data when the additional abundance constraints were not included in the derivation of the fundamental parameters (see §3.1), our estimate of potential systematic errors are $\Delta T_{\text{eff}}/\Delta \log g/\Delta v_t = 125\text{K}/0.25\text{dex}/0.25\text{km}\cdot\text{s}^{-1}$. Imposing the additional abundance constraints, random errors which would still permit a stellar model to satisfy the conditions discussed in §3.1 are $\Delta T_{\text{eff}}/\Delta \log g/\Delta v_t = 50\text{K}/0.15\text{dex}/0.15\text{km}\cdot\text{s}^{-1}$. The additional abundance constraints are most sensitive to changes in T_{eff} (and less sensitive to changes in $\log g$ and v_t) thus, the random errors in T_{eff} are better constrained than the errors in $\log g$ and v_t . We also investigated the differences that using Kurucz (1993) model atmospheres made on our results. These models, in general, satisfied the constraints with slightly lower temperatures (50K at most), lower $\log g$ values (0.1 to 0.2 dex), and lower microturbulent velocities (~ 0.1 km/s), all values within the margin of error we determined for our fundamental parameters.

3.4. Implications of the Model Atmosphere Parameters

As an external check on the the (T_{eff} , $\log g$) pairs determined in the line analyses we compared the adopted gravity of an M4 giant star against that expected from its “evolutionary” position in the c-m diagram. The predicted evolutionary gravity was derived by combining the gravitation law with Stefan’s law, $\log g_{\text{evol}} = -10.564 + 0.4(V - 5\log d - A_V + BC) + 4\log T_{\text{eff}}$, where we have assumed a stellar turn-off and giant branch mass of $0.85M_{\odot}$, a typical value for the main sequence turn-off mass of a globular cluster star (eg. Smith & Norris 1993, Kraft 1994). The symbols have their usual meanings and several standard solar quantities ($\log g = 4.44$, $T_{\text{eff}} = 5772$, and $M_{\text{bol}} = 4.72$) are subsumed in the constant. We calculated evolutionary gravities for a range of recently published M4 distances and extinctions (see Dixon & Longmore 1993 for a review of these values): distances $1.7 \leq d \leq 2.1$ kpc; mean reddening $E(B - V) = 0.37$; and ratios of total to selective extinction [$R \equiv A_V/E(B - V) \simeq E(V - K)/E(B - V)$] in the range of $3.1 \leq R \leq 4.0$. The latter two parameters combine to yield a total visual extinction in the range of $1.18 \leq A_V \leq 1.48$. We interpolated Worthey’s bolometric corrections (1994) as a function of our adopted T_{eff} , $\log g$, and metallicity. We also adopted the formula derived by Cudworth and Rees (1990) to correct for the reddening gradient as a function of coordinate position across the face of the cluster.

In Table 2 we list the evolutionary gravities for each M4 star, assuming that $d = 2.1$ kpc and $A_V = 1.48$. This provided the best overall match between the two gravity sets. If we define $\delta(\log g) \equiv \log g_{\text{spec}} - \log g_{\text{evol}}$, then for this distance/extinction choice $\delta(\log g) = +0.02 \pm 0.01$ ($\sigma = 0.11$). However, other choices of these quantities also yield reasonable agreement. For $d = 2.1$ kpc and $A_V = 1.19$, $\delta(\log g) = -0.16$; for $d = 1.7$ kpc and $A_V = 1.48$, $\delta(\log g) = -0.09$; and for $d = 1.7$ kpc and $A_V = 1.19$, $\delta(\log g) = -0.28$. Only with the assumptions of the closest M4 distance and least interstellar extinction do the spectroscopic and evolutionary gravities clash

badly. Note that a study by Peterson *et al.* (1995) based entirely on kinematical considerations (proper motions and radial velocities) did indeed yield a “short” distance of 1.72 ± 0.04 kpc. However, any mass loss along the RGB would improve the agreement between the gravity estimate based on spectroscopy and that based on kinematical considerations.

Stellar mass loss tracers and/or chromospheric activity indicators can sometimes be observed in the form of core shifts in the Na D lines as well as from circumstellar material in the form of emission in the cores of the Mg II ($\lambda\lambda 2795$ Å) and Ca II *K*-lines, and in the wings of H- α (see *e.g.*, Dupree *et al.* 1992 and references therein). A search of the literature did not uncover any spectroscopic observations of the ultraviolet region of the M4 giants, and unfortunately, the Na D lines on our spectra are affected by telluric emission; a meaningful core shift cannot be measured. However, some of our stars were observed using a wavelength setting that did include the H- α region. We inspected these spectra for H- α emission above the level of the continuum. The results of this exercise are given in Table 3, along with the emission indications reported by other observers (Cacciari & Freeman 1983, Brown *et al.* 1990, Kemp & Bates 1995), for stars in common with our sample. We note whether the emission is observed to the red or to the blue or on both sides of the H- α absorption features. A colon denotes a marginal or weak emission detection. One star, L4611, shows evidence of evolution in the two decades over which its H- α emission behavior has been observed. But, most other M4 giants show little or no evidence for mass loss as indicated by the H- α profiles.

Our model parameters can be used to check ISM extinction properties toward M4. From the T_{eff} values, we estimated intrinsic M4 $B - V$ colors by interpolating the model atmosphere predictions of Cohen *et al.* (1978, their Table 3 and Figure 4). By subtracting these intrinsic $B - V$ colors from the observed colors given in Table 1, we determined the $E(B - V)$ values that are listed in Table 4. Excluding the post-AGB star L1412, we were able to estimate $E(B - V)$ in this manner for all but the two coolest M4 stars observed at high resolution (the Cohen *et al.* model predictions could not easily be extrapolated to the very cool stars L4613 and L4611). Figure 6 shows an angular distribution map of the positions of our M4 program stars on the sky using the $\Delta\alpha$ and $\Delta\delta$ coordinates (as measured from the center of the cluster) from Cudworth & Rees, indicating both Lee’s stellar identifications and our corresponding reddening determinations. The most heavily reddened M4 giants from our analysis lie generally in the western half of the cluster, in good agreement with the differential reddening results of Cudworth & Rees (1990). Our $E(B - V)$ estimates also correlate with IRAS 100 micron fluxes which have been corrected for zodiacal dust contamination.

Lyons *et al.* (1995) also studied the differential reddening across the face of the cluster using interstellar K I column density measurements towards 16 stars, all of which we observed at high resolution. The Lyons *et al.* $E(B - V)$ values are listed in Table 4. Both the mean value and the range of our $E(B - V)$ estimates are in excellent agreement with theirs. Taking the differences in the sense of *this study minus Lyons et al.*, $\langle \delta E(B - V) \rangle = +0.01 \pm 0.01$ magnitudes ($\sigma = 0.05$ magnitude), for 13 stars in common. Another study, by Caputo *et al.* (1985) also derived

mean values of $E(B - V) = 0.32\text{--}0.33$, utilizing an independent method based on the properties of RR Lyrae variables in M4.

We also determined the reddening to the program stars using the dust maps made by Schlegel *et al.* (1998), who reprocessed the high resolution IRAS/ISSA 100 micron maps using the precise COBE/DIRBE calibrations. Surprisingly, the reddening estimates provided from their maps is significantly higher than ours. The difference, for the 22 stars listed in table 4, in the sense of *this study minus Schlegel et al.*, is $\langle \delta E(B-V) \rangle = -0.17 \pm 0.01$ magnitudes ($\sigma = 0.04$ magnitude). This difference cannot wholly be attributed to the assumption of $R = 3.1$ by Schlegel *et al.* Arce & Goodman (1999a) obtained similar overestimates using the Schlegel *et al.* maps in their extinction study of the Taurus dark cloud complex (1999b). In their cautionary note, Arce & Goodman attribute the cause of the reddening (dust opacity) estimate discrepancy to the correlation of intrinsic $E(B - V)$ and Mg_2 assumed by Schlegel *et al.* (90% of the elliptical galaxies used for the regression have low reddenings and the fit is less than good for the few galaxies with $E(B - V) > 0.15$ mag), producing an overall overestimate of reddening values by up to a factor of 1.5 in regions of large extinction. These overestimates agree with those we found for our M4 program stars. In another recent study, Woudt (1998) compares reddening estimates using the Dn-Sigma relation of galaxies in an Abell cluster (ACO 3627) at low galactic latitude with those provided by the Schlegel *et al.* dust maps. In the galaxy studied closest to the galactic plane (WKK5345), Woudt also finds that the Schlegel *et al.* dust maps overestimate the reddening. However, for $E(B - V)$ values of 0.3, values comparable to M4, Woudt did not find any distinguishable difference between the two estimates. Until such time as the cause of the possible overestimation is resolved, we echo the warning issued by Arce & Goodman to use caution when using the Schlegel *et al.* dust maps to estimate reddening and extinction in regions of high extinction.

Because of the methods employed to derive the spectroscopic estimates of reddening, we are able to make star-by-star comparisons of our results against the work done by Lyons *et al.* (1995). For L2206, L2307, and L2406 our reddening estimates are significantly higher than those derived by Lyons *et al.* These three stars are in a region on the sky for which higher than average IRAS 100 μm flux values have also been measured. The stars we observed nearest in the sky to these (*e.g.*, L2208) also have relatively high reddening values. It may simply be that the gas measured in the K I column density measurements—the basis of the Lyons *et al.* reddening estimates—does not completely trace the dust or the IRAS flux measurements, due to shielding effects and variations in the optical depth of the gas as suggested by de Geus & Burton (1991) in their study of the Sco-Oph molecular cloud region.

In addition to large and differential reddening, there is evidence that the dust along the line of sight to M4 has anomalous absorption properties that deviate from the “normal” interstellar extinction law ($R \sim 3.1$; Harris 1973, Schultz & Wiemar 1975, Barlow & Cohen 1977, Sneden *et al.* 1978). Cudworth & Rees (1991), using their photometric observations (by minimizing the spread in V in the HB), found $R = 3.3 \pm 0.7$. Work done by Clayton & Cardelli (1988) gives $R = 3.8$

for σ Sco, a star only one degree in the plane of the sky away from M4. Studying the outer parts of the Sco-Oph dust cloud complex, Chini (1981) proposed $R = 4.2 \pm 0.2$ and Vrba *et al.* (1993) determined $R \simeq 4$ in the nearby ρ Ophiuchi dark cloud. Peterson *et al.* also estimated an $R \sim 4$ for this cluster. Many other investigations, with similarly high R results, are reviewed by Dixon & Longmore (1993).

To examine this issue, we used our T_{eff} values to also estimate intrinsic M4 $V - K$ colors, by again interpolating the model atmosphere predictions of Cohen *et al.* (1978). We compared these predicted values against the observed $V - K$ colors of Frogel *et al.* (1983, their table 17A) after removing the reddening corrections they applied: Frogel *et al.* (1983) had adopted the “classical” values of $E(V - K) = 2.78 \times E(B - V)$. By subtracting the modeled colors from the observed photometry for the thirteen stars in common between our study and theirs, and adding one more star to the list using the $B - V$ photometry of Cudworth & Rees (1990) along with the $V - K$ photometry of Fusi Pecci & Ferraro (1997), we determined color excesses $E(V - K)$ and $E(B - V)$ for fourteen stars in M4, and derived a value of $R = 3.4 \pm 0.4$, in reasonable agreement with those of previous M4 studies.

3.5. Abundance Results

Most abundances were derived as described above, from single-line analyses matching predicted and measured EWs. In addition to employing blended-line EW computations for V I lines, we also used these for determining Ba abundances. The Ba II lines have both hyperfine and isotopic subcomponents, and for these we used the line lists of McWilliam *et al.* (1995). Solar abundance ratios among the $^{134-138}\text{Ba}$ isotopes were assumed in these calculations. In view of our subsequent determinations of large [Ba/Eu] ratios, either a solar system isotopic distribution or one more heavily weighted toward those isotopes generated by s -process neutron-capture synthesis (which would *increase* the Ba overabundances) seems to be appropriate. Finally, full synthetic spectrum computations were used to derive abundances from the $\lambda\lambda 6300, 6363 \text{ \AA}$ [O I], the $\lambda 5711 \text{ \AA}$ Mg I, and the $\lambda\lambda 5682$ and 5688 \AA Na I lines. Comments on most of the abundance computations appear in earlier papers in this series and will not be repeated here. See §3.6 for additional discussion of [O I] line analyses.

In Table 5 we list the final abundances for each star and the cluster mean abundances. Figure 7 presents a “boxplot”, useful for exploratory data analysis, to summarize the mean and scatter of each element. This boxplot illustrates the median, data spread, skew and distribution of the range of values we derived for each of the elements from our program stars. The boxplot also clearly illustrates possible outliers. For example, the abundance ratio range we obtain for proton-capture elements such as sodium and oxygen is quite large. However, the star-to-star abundance variations are very small for all the heavier elements, and for only Ti and V has this result been somewhat pre-ordained.

Table 6 shows the results of numerical experiments to determine the sensitivity of derived elemental abundances to model parameter changes (i.e. potential errors; §3.3). We explored the effects in L2206, a star of intermediate temperature and $\log g$ for which we found $T_{\text{eff}}/\log g/v_t = 4325/1.35/1.55$. The effects of both random and possible systematic T_{eff} errors are shown. For most species, the model uncertainties induce relative abundance errors of less than ± 0.05 dex. The abundances derived from the Fe I lines have somewhat larger sensitivities to microturbulent velocity uncertainties, the Fe II and Mg I lines have larger sensitivities to the derived gravities, and the Ti I and V I lines have the largest sensitivities to the derived T_{eff} .

Figure 8 illustrates the run of Fe-peak and neutron-capture element abundances with T_{eff} . The scatter about the mean (of elements not expected to be sensitive to proton-capture nucleosynthesis) compares well to those obtained in other high resolution cluster work and, as expected, no trend with T_{eff} is observed for these non-volatiles. The abundances of these elements have no apparent trends with RGB or AGB position, since there are no perceptible slopes with T_{eff} depicted in Figure 8. Sneden *et al.* (1997) have found large (~ 0.4) scatter in $[\text{Ba}/\text{Fe}]$ and $[\text{Eu}/\text{Fe}]$, with $\langle [\text{Ba}/\text{Eu}] \rangle \sim -0.4$ among 18 M15 giants, but that obviously is not seen in our M4 sample, in which $\langle [\text{Ba}/\text{Eu}] \rangle = +0.60 \pm 0.02$ ($\sigma = 0.10$); the scatter here is probably dominated by observational/analytical uncertainties.

Usually, calcium abundances are sturdy enough to also be included in a plot such as Figure 8. However, the scatter in the derived calcium abundance ($\sigma = 0.11$) is a little larger than that expected due to observational error alone and demands further investigation. Previous work using similar analysis techniques on data of comparable resolution and sample size include those of M13 by Kraft *et al.* (1997) and M15 by Sneden *et al.* (1997) for which 18-star samples of calcium abundances show $\sigma = 0.03$ and 0.05, respectively. Simply eliminating calcium lines that had not been included in previous Lick-Texas cluster analyses did not decrease the variation in the abundance results. We also investigated the possibility that uncertainties in EW measurements, combined with our choices in microturbulent velocities, could result in the derived calcium abundance variations. However, seven of the calcium lines we use are in common with those of Drake *et al.* (1994), who studied four stars in common with our sample. For the 18 calcium line measurements in common between the two studies (where the average EW is ~ 85 mÅ), we find a mean difference in the sense *this study minus Drake et al.* of 3.3 ± 1.4 mÅ. And, although our mean abundance for these stars is slightly offset from their study (Drake *et al.* adopted systematically higher surface gravity values but found similar microturbulent velocities), the relative range of difference in the four-star sample is approximately the same, with ours slightly more restricted (we find a total calcium abundance range of 0.08 for these four stars and Drake *et al.* find 0.13). We also compared our abundance results for the three giant stars we studied in common with Brown & Wallerstein (1992): we find a mean difference in the sense *this study minus Brown & Wallerstein* of 0.02 dex, with two of the stars showing much lower than average Ca abundances in both studies.

M4 stars are known to have a range of CN-strengths. We find that the scatter in our calcium

abundances seemed to correlate with the CN-strength of our stars: the calcium difference, in the sense of $[Ca/Fe]_{CN-Strong} - [Ca/Fe]_{CN-Weak}$ shows a large scatter, 0.08 ± 0.11 dex. Drake *et al.* (1994) also found that their “calcium results suggest that this element might be slightly more abundant in the CN-strong stars than in the CN-weak stars”. They investigated the possibility that stronger calcium lines may be the result of cooler outer envelopes that have large cyanogen opacities. They found that atmospheric temperature effects due to differential molecular blanketing are not responsible for abundance variations of Na, Al, O, or Ca. While upper atmosphere cooling *can* produce correlations between Na and Al abundances with CN-strengths, a corresponding correlation would be expected in the resonance lines of neutral potassium which is even more sensitive to upper atmosphere cooling (K I has a lower ionization potential than either Na I or Al I). However, no such correlation was found for the two pairs of CN-strong and CN-weak M4 stars investigated by Campbell & Smith (1987). While none of their stars overlap our high resolution sample, we are able to verify, using the λ 7699 Å K I line which appears in a telluric-free region redward of the A-band on our program star spectra, that there is no difference in K I strength between the CN-strong and CN-weak pairs in our sample.

Finally, we tested whether the scatter in the Ca abundance might be due to an inability of our EW analysis to properly account for CN-blending in the spectra of the CN-strong stars: we looked for the problem to appear in EW analyses of other elements *known* to be affected by CN, such as oxygen. However, a comparison of the scatter in the oxygen abundance results between those obtained by the EW analysis procedure ($\sigma = 0.15$) with those obtained by spectrum synthesis ($\sigma = 0.14$) shows no significant difference in the dispersion of values obtained by both methods and reveals only the expected offset due to the proper accounting of CN-blending in the synthesized spectrum. Despite the preceding tests, we are not satisfied that the scatter is of nucleosynthetic origin: most of AGB stars are also CN-weak stars (this is discussed further in §4.2.3) and we note that a 50K upward revision in temperature (see Table 6) would increase the Ca abundance in these stars to match that of the CN-strong RGB stars.

In Table 7 we restate our mean M4 abundances, combining the results for the two ions of Fe and Ti as straight averages. We also tabulate the abundances of Gratton *et al.* (1986), Brown & Wallerstein (1992), and Drake *et al.* (1992). For contrast, we also list mean abundances in M5, in typical field metal-poor stars, and also the very metal-poor cluster M15. For this simple overview we chose not to break down the comparisons on a star-by-star basis; only cluster means are considered. Even with this limitation, it is clear that our M4 abundances generally agree well with those of past M4 investigators. The M4 abundances of non-volatile elements Ca, Sc, Ti, V, and Ni also are in good accord with those in M5 and the halo field (again with the warning that Ti and V abundances have been partially forced to this conclusion). The *r*-process neutron-capture element Eu also has essentially the same mean abundance in M4, M5, M15, and the field stars. Our M4 average Na and Si abundances are substantially larger than those of M5 and the halo field stars but agree with those of the very metal-poor cluster M15. But all M4 analyses agree on this point. The elevated Na and Si abundances will be explored further in §5

The only M4 abundance disagreement substantially in excess of observational uncertainties (typically ~ 0.1 in $[\text{el}/\text{Fe}]$ ratios) is with the Gratton *et al.* (1986) Ba abundance. Both we and Brown & Wallerstein derive $[\text{Ba}/\text{Fe}] \sim +0.6$, while Gratton *et al.* suggest that this ratio is ~ 0 , about the solar system ratio. This single discrepancy cannot be resolved here, as we have no high resolution spectra for the three M4 stars (L1605, L2608, and L2626) of the Gratton *et al.* sample. But, if we and Brown & Wallerstein (1992) are correct about the mean Ba abundance in M4, this element is extremely overabundant with respect to the comparison samples.

Some comment must be made on the reliability of the Ba and Si abundances in our study. Not only do our results for Ba agree with those of Brown & Wallerstein, they are also in accord with those derived for quite different M4 stars by Lambert *et al.* (1992). Lambert *et al.* obtained $[\text{Ba}/\text{Fe}] = +0.50$ and $+0.63$ in two blue HB stars, using lines of intermediate strength. However, we caution the reader that our Ba abundances are derived from very strong lines and thus are extremely sensitive to adopted microturbulent velocities. We can lower the $[\text{Ba}/\text{Fe}]$ by ~ 0.3 dex simply by increasing our microturbulence velocities by a very large amount: $\sim 1.0 \text{ km s}^{-1}$. But, doing so produces unforgivably large trends of Fe I line abundances with EWs. The v_t we chose for each star was in accord with the abundance indications we used to determine the final T_{eff} and $\log g$ parameters we adopted for the models. Our estimate of the random error of the microturbulence velocities, based on the dependence of Fe I line abundances with EW, is 0.15 km s^{-1} , too small an error to explain away the very large Ba abundances we derived. However, without Ba I lines in our spectrum or weaker Ba II lines for which the atomic parameters are well known, there is no resolution to the dilemma at this time. We hope to resolve the issue in a future investigation by comparing this element, and other *s*-process element abundances, against those derived for M5 stars of similar T_{eff} , $\log g$, and metallicity observed with the Keck HIRES.

We have confirmed the apparent excess of *s*-process species in M4 using the relatively weaker lines of lanthanum. We derived La II abundances using the CN-free line at $\lambda 6774.33\text{\AA}$ and, especially in the cases involving the hotter, higher $\log g$ stars (where the line was very weak), checking to ensure that the result was in reasonable accord with results derived from $\lambda\lambda 5808.31$ and 6390.49\AA (CN-blended lines). Although literature values of La abundances are sparse for metal-poor stars, Table 7 shows both the excellent agreement we obtain with previous work in M4 (Brown & Wallerstein 1992) as well as the overabundance of La as compared with field halo giants of comparable metallicity.

While our silicon abundance results are in good agreement with previous studies of M4, they are significantly higher than the abundances found either in M5 or in the field. Unlike the Ba II lines used in our analysis, the Si I lines are all of intermediate or weak strength, with very little sensitivity to random errors in the fundamental parameters of the stellar models. Comparing our EW measures of the Si I lines against those made available by J. Brown (1998), the EWs of these lines show the same average offset and scatter as the rest of the sample. However, high Si abundances are seen in the very metal-poor cluster M15 and are thus not unprecedented among globular clusters. Further exploration of this issue is postponed to §5.

3.6. Carbon and Nitrogen Abundances

Our M4 spectra did not contain spectral features suitable for independent determination of carbon and nitrogen abundances. But, by making use of previous investigations of these elements we were able to compute total abundances of the CNO group. Since the [O I] $\lambda\lambda 6300, 6363\text{\AA}$ lines are blended with CN, we also explored the effects of the adopted C and N abundances on the derivation of oxygen abundances. Finally, C and N abundances were also employed in deriving $^{12}\text{C}/^{13}\text{C}$ ratios, using the CN red system features near 8000\AA .

Suntzeff & Smith (1991, hereafter SS91) used low resolution ($R \sim 2000$) CTIO IRS spectra of first-overtone vibrational bands of CO near the $2.3\mu\text{m}$ to determine C abundances for 32 M4 giants. With only CO band observations at hand, their derived C abundances were not formally independent of assumed O abundances. They assumed a uniform oxygen overabundance of $[\text{O}/\text{Fe}] = +0.3$ in synthetic spectrum computations of the CO bands. This is slightly larger than the mean abundance found in our study: from Table 5, $\langle [\text{O}/\text{Fe}] \rangle = +0.25 \pm 0.03$ ($\sigma = 0.14$). However, since C is always at least a factor of 10 less abundant than O in M4 giants, the CO strength is almost entirely controlled by the available C atoms. SS91 did explore the effect of reducing their assumed O abundance by 0.3 dex and found that the derived C abundance changed by less than 0.1 dex. Thus no adjustment in their C abundance scale was deemed necessary for this potential source of uncertainty.

We paid more attention to model atmosphere parameter differences with SS91. We have 12 stars observed at high resolution that are in common with their work. They assumed lower temperatures, higher gravities, as well as higher microturbulent velocities than we did. Employing our fundamental parameters would yield systematically higher abundances; the biggest C abundance effect comes from a combined temperature/gravity shift. We therefore adjusted their C abundances to our temperature scale by doing a least squares fit in T_{eff} to their data set (excluding one large outlier) using standard linear regression techniques, and used this function to calculate the difference in assumed C as a function of temperature. In Table 8, we tabulate the SS91 C abundances and the adjusted values, and in Figure 9 we plot their C abundances as a function of T_{eff} for 29 stars, excluding the anomalous L1412. The C abundances tend to decrease with decreasing T_{eff} ; this probably is the result of increased mixing of CN-cycle material to the stellar surfaces as M4 stars ascend the RGB. For the 12 stars in common with us (solid circle symbols) we also show arrows to the adjusted $\log \epsilon(\text{C})$ values at the higher T_{eff} 's derived in this study.

Using these C abundances, we calculated synthetic spectra for portions of the CN red system $A^2\Pi-X^2\Sigma^+$ (2-0) band near $\lambda 8000\text{\AA}$, and derived N abundances. For the synthetic spectra we adopted the atomic/molecular line lists of Gilroy (1989). In Table 8 the N abundances determined in this manner are given, and the O abundances for all of our “high-resolution” stars from Table 5 also are retabulated here in $\log \epsilon(\text{el})$ form.

The derived mean M4 giant star C abundance is $\langle \log \epsilon(\text{C}) \rangle = 6.81 \pm 0.07$ ($\sigma = 0.25$), or

$\langle [C/Fe] \rangle = -0.57 \pm 0.07$,¹³ and the derived mean N abundance is $\langle \log \epsilon(N) \rangle = 7.62 \pm 0.13$ ($\sigma = 0.47$), or $\langle [N/Fe] \rangle = +0.75 \pm 0.13$. Our results compare reasonably well with two other studies of C and N in M4. Brown *et al.* (1990), employing spectrum synthesis of CH features of the $A - X$ system in the blue wavelength region, obtained $\langle \log \epsilon(C) \rangle = 6.97 \pm 0.06$ for their three non-peculiar stars. Adopting this C abundance, they then obtained their N abundance of $\langle \log \epsilon(N) \rangle = 7.83 \pm 0.15$ by doing an equivalent width analysis of (2–0) band lines of the CN red system. Smith & Suntzeff (1989), using low resolution ($R \sim 2000$) KPNO FTS spectra taken of first-overtone bands of CO in the K -band near $2.3\mu\text{m}$, derived the C abundance for seven M4 stars, six of which are in common with this study. Excluding the peculiar star L1412, the average C abundance they obtained is $\langle \log \epsilon(C) \rangle = 6.75 \pm 0.23$.

The C+N+O abundance sums are also given in this table. They are constant to within the analysis uncertainties, with a mean value of $\langle \log \epsilon(C+N+O) \rangle = 8.24 \pm 0.03$ ($\sigma = 0.09$). This is just the total C+N+O one would expect if the material out of which the M4 giants formed was enhanced in O over the scaled solar abundance by $[O/Fe] \simeq +0.4$, as is expected from previous work on metal-poor globular clusters.

The derived or extrapolated C and N values were then adopted in the $\lambda\lambda 6300, 6363\text{\AA}$ regions where the oxygen abundances were determined by spectrum synthesis. Some trials were made, adjusting the C and N abundances up and down but keeping the total of $[C/Fe]$ plus $[N/Fe]$ abundance (hereafter C+N) constant. The oxygen abundance, at least to the level of accuracy that can be determined with these data, did not depend on the relative ratios of $[C/Fe]$ to $[N/Fe]$, just the total C+N. This is because the CO association is relatively small in the CN line-forming layers of the M4 RGB stars, and thus C is mostly in the neutral atomic state. A decrease in either C or N abundance therefore must be compensated by an increase in the other atom in order to keep CN line strengths approximately constant. Other numerical experiments we performed showed that changing the C or N abundance alone, and holding the other values fixed, made less than one percent difference in the depths of the modeled $[O\text{ I}]$ profiles.

3.7. The $^{12}\text{C}/^{13}\text{C}$ Ratio

We also determined carbon isotope ratios $^{12}\text{C}/^{13}\text{C}$ for our program stars. The dissociation potentials of CN and CO molecules are not sensitive to isotopic substitution. Thus, we assumed that the number-density ratio of ^{12}CN to ^{13}CN molecules was equal to that of the isotopic abundance ratio $^{12}\text{C}/^{13}\text{C}$. The ratios were determined using spectrum synthesis of portions of the (2–0) band of the CN red system near $\lambda 8005\text{\AA}$. Once the N abundance had been determined from ^{12}CN features for a constant assumed isotopic ratio, the nitrogen abundance was fixed and the

¹³Here we have assumed the solar CNO abundances of Anders & Grevesse (1989): $\log \epsilon(C) = 8.56$, $\log \epsilon(N) = 8.05$, and $\log \epsilon(O) = 8.93$.

ratio was allowed to vary. A best fit to the data was determined by eye. The derived $^{12}\text{C}/^{13}\text{C}$ value for each program star is given in Table 8, followed in parentheses by the minimum and maximum possible values that the fitting procedure would allow. The average ratio obtained for our program stars is $\langle^{12}\text{C}/^{13}\text{C}\rangle = 4.5 \pm 0.1$ ($\sigma = 0.6$).

The $^{12}\text{C}/^{13}\text{C}$ ratio, based on a comparison of line intensities originating in similar or identical rotational and vibrational levels, is insensitive to errors in adopted effective temperatures, surface gravities, line oscillator strengths, and molecular dissociation energies (see the discussion in Lambert & Sneden 1977), making it a robust indicator of the presence of CNO-cycle processed material. We investigated the effect on the abundance ratio resulting from possible errors in our N abundance determinations only to verify that the iterative approach we used to obtain the isotope ratio and assumed N abundance is a self-correcting one, assuming some fixed value for the C abundance.

Our results fall within the range of values found by Brown & Wallerstein (1989) and SS91 for the stars in common. This excellent agreement with previous studies confirms from CN red system syntheses the extremely low carbon isotope ratios found from the CO bands. For the evolutionary domain of our program stars, there is no obvious trend of $^{12}\text{C}/^{13}\text{C}$ ratios as a function of giant branch luminosity.

3.8. The CN-Strong, CN-Weak Dichotomy: A New CN-Strength Index

M4 has a well-developed CN-strong, CN-weak dichotomy which we propose to discuss in relation to the carbon, nitrogen, and oxygen abundances derived from the present observational material. We observed 14 stars at high resolution in common with either Norris (1981) or SS91, who determined CN strengths for these stars using S(3839) indices (measures of the ratios of the flux intensities of the cyanogen band near 3839 Å). However, this left ten stars in our high resolution sample for which a CN classification was unknown. While the signal-to-noise of our spectra in the red is quite good, the flux in the blue is too poor to independently determine either the carbon abundances from the CH G-band, or the S(3839) CN-strength index. In order to investigate the dependence of other light element abundances on the CN strengths of all our stars, we developed a simple CN-strength measure from the CN (2–0) bandhead at 7872 Å. In Figure 10 we show the appearance of this bandhead in M4 program stars with varying amounts of CN absorption. We determined a “bandhead” EW via a straight numerical integration of the total absorption in the wavelength region $\lambda 7872.4\text{--}7876.4$ Å. This EW, which we call EW7874, covered several CN lines, and this provides a measure of the CN-strength for the stars in our high resolution sample.

Figure 11 shows our EW7874 measure as well as the S(3839) index as determined by either Norris or SS91, as a function of V magnitude. The baseline for the S(3839) plot is from Norris. As illustrated in the figure, there is a variation in the CN-strength with magnitude, regardless

of which measure is used. Stars on the giant branch have correlated color and magnitudes: some of the CN-strength we measure in EW7874 arises from temperature effects, with the cooler stars showing stronger molecular features in general. However, we were unable to independently determine the T_{eff} baseline for EW7874 using our relatively smaller sample of stars. Instead, the T_{eff} baseline for EW7874 was obtained by taking advantage of the previous work done by Norris and SS91, adopting the linear slope in T_{eff} which provided the best resulting correspondence with the previous designations for those stars we observed in common. Then, the relative CN-strength values for all stars were determined as offsets from this line:

$$\delta\text{EW7874} \equiv \text{EW7874} - (165.784 - 0.025 \times T_{\text{eff}}).$$

The values δEW8984 , our adopted parameter of the CN strength for all of our high resolution stars, as well as the published values of S(3839) for the stars in common, are given in Table 8. We find only two mildly discrepant points (L1408 and L2206), for which we determine intermediate CN-strengths but Norris and/or SS91 designate as strong, according to their blue CN index. Both stars are among those in our $R \sim 60,000$ sample; continuum placement is not a problem. Telluric lines in the EW7874 region are shown in Figure 10 and one would require a much too large over-division of the telluric lines in order to explain the weakness of the red index. However, the indices for the remainder of the stars in common are in good agreement.

By placing the red EW7874 estimate, in effect, on the S(3839) system, we are now able to give CN-strength designations to all of our stars observed at high resolution: we will denote stars as either CN-weak ($\delta\text{EW7874} \leq 64$) or CN-strong ($\delta\text{EW7874} \geq 86$) in the remaining plots that follow in our discussion. But here we alert the reader to two caveats about this scheme. First, adoption of this two-bin CN-designation deliberately avoids finer grouping distinctions of stars with intermediate CN strengths. For the purposes of this discussion, the coarser CN-strong/CN-weak notation will suffice. Second, we do not have an equal number of CN-weak and CN-strong stars. To assume so would have forced us to choose a lower EW7874 value for the division. Of the stars with the highest δEW7874 values we have designated as CN-weak, the spectra are all similar in appearance and to distinguish, by number alone, CN-strong versus CN-weak among these stars would be misleading. Instead, we have taken advantage of the previously determined CN-strengths assigned from the S(3839) system, as well as the distinctions we can discern both by eye and by measure in the EW7874 region, rather than make the designations blindly, by raw number alone.

3.9. Medium Resolution Abundances

We determined only oxygen abundances from the medium resolution Argus spectra (Table 9). We first analyzed the stars in common with the high resolution observations, using the previously determined T_{eff} , v_t , $\log g$, and overall metallicity [Fe/H] values. In §2.2 we explained the procedures used to eliminate the major telluric O_2 contamination that plagues the $\lambda 6300 \text{ \AA}$ region of the Argus spectra. During the O abundance analysis this issue was revisited, and the results of

the [O I] syntheses were tested for the effect of different choices in telluric line division. Since the Argus multi-object spectrograph observed all of the program stars at the same time through the same air mass, after these numeric experiments we applied the telluric line removal procedure in a consistent manner to all Argus stars. Despite the telluric line removal complication caused by the known resolution change across the fibers (§2.2), the agreement of O abundances between the medium and high resolution data sets is excellent. Taking the difference in the sense *high resolution minus medium resolution*, $\langle \delta[\text{O}/\text{Fe}] \rangle = -0.01 \pm 0.02$ ($\sigma = 0.07$, for 13 stars in common).

For the remaining eleven stars, we adopted the mean metallicity of M4 ($[\text{Fe}/\text{H}] = -1.18$) and a microturbulent velocity $v_t = 1.75 \text{ km s}^{-1}$. This v_t is the mean of the warmer stars observed at high resolution with $T_{\text{eff}} > 4325 \text{ K}$ (a temperature no cooler than the lowest predicted T_{eff} of the medium resolution sample). In deriving the stellar temperatures, we again utilized the “Gray” method, but calibrated the ratios using the results we obtained using the high resolution spectra. The wavelength coverage of the medium resolution data includes five of the lines we had previously measured and used to derive the initial temperature rankings of the high resolution data. At this resolution however, all of the lines were blended, and two original Gray ratios proved to be useless for these data and were eliminated. The remaining three lines, not as severely blended, formed two pairs; we measured the line depths for these lines. The logarithmic line depth ratios were fit as a second-order polynomial function to the corresponding temperatures and the inverted form of this function was used to predict the temperatures of the remaining stars. For only one star (L1617) was an extrapolation required based on its depth ratio. We calculated an evolutionary gravity for each star, adopting the distance (2.1 kpc) and extinction ($A_V = 1.48$) that had produced the best match between the spectroscopic and evolutionary gravities found earlier from the high resolution data. We adopted cluster mean abundances in the synthetic spectrum computations, and resulting [O/Fe] values for these 11 medium-resolution-only stars are given in Table 9.

4. M4 Nucleosynthesis

In this section we examine the probable causes of the abundance trends found in our study. We first summarize the main observational results emerging from the previous sections. From this large data set we have found the following:

1. The Fe metallicity of M4 is $\langle [\text{Fe}/\text{H}] \rangle = -1.18$ ($\sigma = 0.02$) for the 23 M4 stars observed at high resolution, excluding the pathological star L1412 and the possible binary L2406 (see §4.1). The dependence of the metallicity on analysis assumptions has been discussed in §3; this probably adds an additional scale uncertainty of less than ± 0.10 to the scatter about the mean quoted here.
2. The deduced reddenings, total extinctions, and cluster distance are reasonably consistent with previous investigations. Our analysis confirms the earlier claims of star-to-star extinction variations, with a generally increasing trend seen across the face of the cluster,

from east to west. The total-to-selective extinction ratio is larger than the typical ISM value, again in agreement with the work of prior investigators.

3. Abundance ratios with respect to Fe typical of halo field and cluster stars are obtained for Sc, Ti, V, Ni, and Eu. The star-to-star abundance variations in all these elements are $<\pm 0.1$ (from the σ values in the $[X/Fe]$ ratios).
4. Very high relative abundances for Si and Ba are obtained in our study ($[Si \text{ or } Ba/Fe] \sim +0.6$), as well as high La ($[La/Fe] \sim +0.5$) which echo the results of the earlier investigation by Brown & Wallerstein (1992). High Si abundances, although not common among globular cluster giants, have also been found in the very metal-poor cluster M15.
5. Star-to-star variations in the proton-capture elements O, Na, and Al are detected. Al is overabundant in all M4 giants: $\langle [Al/Fe] \rangle \gtrsim +0.4$.
6. Substantial enhancement of N abundances is deduced ($\langle [N/Fe] \rangle \sim +0.7$) that accompanies often large C depletions ($\langle [C/Fe] \rangle \sim -0.6$). The carbon isotope ratio is also extremely low in all stars of our sample. Although several M4 giants exhibit oxygen deficiencies, most M4 giants show little evidence for severe O depletions ($\langle [O/Fe] \rangle \sim +0.25$), such as are seen in M13 (Kraft *et al.* 1997) and M15 (Snedden *et al.* 1997). Excluding the two coolest program stars (for which we place large uncertainties on our abundance results), only three stars have $[O/Fe] \leq +0.10$. With the caution that the derived C, N, and O abundances have substantial analysis uncertainties, we conclude that the C+N+O abundance sum is constant to within the observational errors, and agrees with the C+N+O total that might be expected for M4 stars at birth.

4.1. An H-R Diagram for M4 Giants

Interpretation of our abundance data requires knowledge of the evolutionary states of the M4 program stars. The variably-reddened ($V, B - V$) c-m diagram of Figure 1 is clearly inadequate for this task, so in Figure 12 we display an (M_{bol}, T_{eff}) H-R diagram whose quantities are based on our spectroscopic results. The abscissa T_{eff} values are those of Table 2. The ordinate M_{bol} values have been computed from the V magnitudes of Table 1, derived $E(B - V)$'s from Table 4, bolometric corrections BC from Worthey (1994), and the true M4 distance modulus ($m - M$) = 11.61 (from our preferred distance $d = 2.1$ kpc). For these choices of d and A_V , the brightest M4 stars have $M_{bol} \sim -3.5$, a value which agrees well with the theoretical M_{bol} (~ -3.55) expected at the He core flash (*e.g.* Rood 1972, Sweigert & Gross 1978).

In Figure 12 the RGB tip is clearly defined, as is the AGB split from the lower RGB. Note that a comparison of Figures 1 and 12 emphasizes that the number of M4 AGB stars *observed* in our survey overrepresents their true numbers relative to lower RGB stars. This is entirely an artifact of our magnitude-limited high resolution sample. The defect is partially repaired in our

medium-resolution sample, which has about eight lower RGB stars. For nearly all program stars, the derived H-R diagram illustrates far less scatter than the observed c-m diagram.

One anomalous star stands out in Figure 12: L2406, alias V13. It is variable in spectral type (G3–K0, Joy 1949), and in V magnitude (12.4–13.1, Sawyer Hogg 1973; see also Lloyd Evans 1977). Our analysis yielded a $(\log g, T_{\text{eff}})$ combination which, when convolved with the observed V magnitude and our predicted $E(B - V)$, produces a star with the anomalously bright M_{bol} depicted in Figure 12. The appearance of the L2406 spectrum is in fact very similar to two other fainter stars we found in the same $T_{\text{eff}} \simeq 4100$ K range, but the microturbulent velocity proved to be unusually high. Closer inspection of the spectrum revealed that its absorption lines are much broader than those of other M4 giants, and are slightly blueward asymmetric. It is thus possible that L2406 is a close physical (or line-of-sight) binary consisting of two giant stars of similar magnitude and temperature. A binary interpretation would not itself explain the photometric and spectral type variability of this star, but a comprehensive investigation of the nature of L2406 is beyond the scope of this paper. The star will be excluded from further discussion and interpretation of our M4 abundance results.

4.2. Tests of Proton-Capture Nucleosynthesis

Armed with a rectified M4 upper giant branch H-R diagram and CN-strength indices for essentially all of the stars from our high resolution sample, we investigate the abundances of those elements that are sensitive to proton-capture nucleosynthesis (via the CN-, ON-, NeNa- and MgAl-cycles): carbon, nitrogen, oxygen, sodium, magnesium and aluminum. We consider the relationship of these abundances first to each other and then to evolutionary state.

4.2.1. C, N, and O

Figure 13 illustrates the relationship between C and N versus O for the 12 stars of Table 8 for which all three elements have abundance measurements (recall from §3.3 that the open square symbol, \square , here and in subsequent figures, refers to a high luminosity, low T_{eff} star for which model parameters and abundance determinations are relatively uncertain). The distribution of points is compatible with a proton-capture scenario: low oxygen abundances are accompanied by low carbon and elevated nitrogen. The more highly CNO-processed stars are usually also the CN-strong stars. In addition, the sum of C+N+O is essentially constant, as expected, if all stars draw on the same primordial material. Note also the existence of one star (L4201, observed at slightly lower resolution, $R \sim 30000$, than the bulk of our high resolution sample), in which O appears to have remained undepleted, whereas C \rightarrow N conversion has taken place, which suggests that the material of this star has been subjected to less-advanced nucleosynthetic processing than has been the case for the other stars of our sample.

4.2.2. Na and Al vs. O; Mg and Al vs. Na

In Figure 14, we plot sodium and aluminum abundances *vs.* oxygen. The anticorrelated behavior of Na relative to O, common among giants in many other globular clusters (*e.g.* Suntzeff 1993, Briley *et al.* 1994, Kraft 1994, Wallerstein *et al.* 1997), is clearly seen. Less striking is the apparent anticorrelated behavior of Al and O. These anticorrelations exhibit some of the characteristics of the proton-capture deep-mixing scenario (Langer *et al.* 1993, Langer & Hoffman 1995, Langer *et al.* 1997, Cavallo *et al.* 1998) in which Na and Al are enhanced in the stellar envelope at the expense of Ne and Mg, respectively, as the envelope is circulated through the hydrogen-burning shell. As is seen in Figure 13, the CN-strong stars are those that are more highly processed via proton-capture syntheses. The CN-strong group has a mean Na abundance that is a factor of two larger than the CN-weak group: $\Delta[\text{Na}/\text{Fe}] = 0.32 \pm 0.06$. Correlated Na and CN variations are also observed in a few pairs of stars in NGC 6752 (Briley *et al.* 1999), a cluster of comparable metallicity to that of M4. Our CN-strong group also has higher Al abundances but the CN-strong/CN-weak difference is much less pronounced: $\Delta[\text{Al}/\text{Fe}] = 0.16 \pm 0.05$. This situation is the reverse of that found in M13, in which the range in Al abundances far exceeds that of Na (Kraft *et al.* 1997).

Two stars stand out which do not completely follow the trends exhibited in Figure 14: L4201 and L2208. We noted already that L4201 has an anomalous position in Figure 13, which indicates that, whereas C has been converted to N, O remains unchanged. The fact that Na is enhanced in this star whereas Al remains relatively low is consistent with theoretical predictions (Langer *et al.* 1997, Cavallo *et al.* 1998) which argue that, in a hydrogen-burning shell, Ne can be transmuted to Na when C is transmuted to N, even though the shell temperature is too low to permit O \rightarrow N conversion, and much too low to convert ^{24}Mg to Al. The star L2208 is, however, anomalous if we require that all stars in M4 should begin their evolution with identical [el/Fe]-ratios. It is CN-strong (Table 8) and has the highest $^{12}\text{C}/^{13}\text{C}$ ratio in our sample (although it still approaches the equilibrium value). At the same time, it has relatively high abundances of O, Na, Mg and Al. We note that this one star defines the highest point in four of the elements shown in the boxplot (Figure 7) and that its abundances are in the upper quartile for yet four other elements. Star L2208 also resides in a "special" place on the ($M_{\text{bol}}, T_{\text{eff}}$) H-R diagram (Figure 12), assigned to neither the AGB nor RGB. Unfortunately, L2208 is among the stars we observed at slightly lower resolution ($R \sim 30000$), and, in this case, slightly lower signal-to-noise. Nevertheless, it is possible that *this* star began with larger abundances of the α - and light odd elements than its cluster companions and that it has undergone only rather modest deep-mixing, sufficient only to drive the $^{12}\text{C}/^{13}\text{C}$ ratio toward the equilibrium value. The existence of stars exhibiting primordial differences in the light element abundances would not be unique to M4. For example, correlated CN and Na variations are seen in stars near the main sequence of 47 Tuc (Briley 1997). And, in M5, star IV-59 has a total C+N+O abundance exceeding that of any other analyzed giant in the cluster (Snedden *et al.* 1992, Smith *et al.* 1997).

In Figure 15, we illustrate the correlation between Na and Al as well as the lack of one between

Mg and Na (note the anomalous position of L2208, which we ignore for purposes of the subsequent discussion). If Na and Al are correlated, and if we assume that the Na enhancements are a result of proton captures on Ne, then one would suppose that the Al enhancements must be a result of proton captures on Mg, yet Mg seems unchanged. However, if we assume that the Al “floor” for all M4 stars corresponds to those we observe having the lowest Al abundances ($[Al/Fe] = +0.4$, corresponding to $\log \epsilon(Al) \sim 5.7$), then the Al enhancement required is +0.4 dex. The “highest” Mg abundances we see is about $[Mg/Fe] = +0.5$ (corresponding to $\log \epsilon(Mg) \sim 6.9$): the Mg abundance would need to drop by only about 0.05 dex to account for the increase in the abundance of Al. This change is too small to be detected with certainty from the present observational material. Such a change *may* be compatible with theoretical expectation, if scaled solar values for the isotopic ratios of $^{24}Mg/^{25}Mg/^{26}Mg$ are invoked in the case of M4 (78.99:10.00:11.01, de Bièvre & Barnes, 1985).

As shown by Langer & Hoffman (1995, their Fig. 1), very modest hydrogen depletion of the envelope material ($< 3\%$) can lead to an enhancement of Al by +0.4 dex when Na is enhanced by +0.7 dex, exactly as observed in our M4 sample. In this picture, the enhancement of Al comes about entirely by destruction of ^{25}Mg and ^{26}Mg : ^{24}Mg remains untouched. Proton-capture on the lesser isotopes of Mg can occur at lower temperatures ($T_9 \sim 0.04$) than on ^{24}Mg ($T_9 \sim 0.07$). It is unclear whether the scaled solar values are appropriate in the case of the lesser isotopes of Mg. There is evidence (Tomkin & Lambert 1980, Barbuy 1985, Lambert & McWilliam 1986, Gay & Lambert 1999) for a reduction in the abundances of the rare isotopes of Mg relative to ^{24}Mg in ~ 20 to 30 metal-poor stars. On the other hand, Shetrone (1996b) found solar-like ratios of $^{25}Mg+^{26}Mg$ to ^{24}Mg among giants in M13, where the star-to-star abundance variations in Mg are found to be a result of processing ^{24}Mg into Al. We attempted to determine this in our M4 stars by performing spectrum synthesis of the Mg isotope ratios in the MgH region near $\lambda 5140$ AA, adopting the line lists of Gay & Lambert (1999). There is a redward asymmetry of the MgH lines that seems to be better modelled by a solar or slightly supersolar Mg isotopic ratio than a subsolar one. While it is tempting to interpret this as a similarity in the Mg isotopic ratio behaviour between the giant stars in M4 and M13 where the cluster star behaviour is different from that found in the field, higher signal-to-noise data and, more importantly, higher resolution data, perhaps of $R \sim 120,000$, are required to determine the isotopic ratios of the M4 stars with complete confidence.

4.2.3. *C,N,O Abundances as a Function of Evolutionary State*

The Na *vs.* O and Na *vs.* Al correlations among the M4 giants permit us to comment on the possible evolutionary dependence of proton-capture element abundances to the C,N,O group. The range of bolometric magnitude over which we have a “pure” sample of either RGB or AGB stars is not large (~ 1 mag.), and the two branches cannot be distinguished when $M_{bol} < -2.0$ (see Figure 12). Consequently, we confine our attention to an RGB group of 11 stars, the brightest of

which is L3612, and an AGB group also consisting of 11 stars, the brightest of which is L2206. Presumably, the AGB stars represent a stage of evolution more advanced than the RGB stars; we treat the groups as “single” entities, without any attempt at further subdivision. We designate L1408 and L2206 as “CN-weak” in accordance with their EW7874 values, even though previous investigations based on the blue CN-bands referred to them as “CN-strong”. In this exercise, we also deleted L2208, a star which we had already concluded has anomalously high primordial abundances of the α - and light odd elements (see §4.2.2).

We note here that the AGB population is over-represented in our sample relative to the RGB, since stellar evolutionary theory indicates that the AGB lifetime is only about 20 percent that of the RGB. This comes about entirely as a result of observational selection: in a spectroscopic survey, one tends to choose the brighter stars first. However, this should have no effect on the conclusions reached here, since the AGB and RGB samples are surely large enough to be representative of their evolutionary states.

Although oxygen abundance estimates are available for all 22 of these stars, carbon and nitrogen abundances are available for only six of them. However, all but four (all on the RGB) have CN-strength designations. We therefore explore the question of what combination of C,N,O abundances governs the CN-strong and CN-weak designations, on the basis of all ten stars for which C,N,O abundances are available (excluding L1514 and L2406 as discussed in §3.3 and 4.1) in Table 8. In Figure 13, all CN-strong stars have C depleted and N enhanced. If CNO processing occurs, O depletion will be accompanied by C depletion, which is also seen in Figure 13. And, the position of L4201 shows that it is possible to have a star in which O is not depleted, but still is CN-strong if C has been converted to N. CN-weak stars seem to be driven almost exclusively by the low abundance of N, with C taking on almost any value. The low abundance of N, in turn, is controlled largely by the absence of significant O \rightarrow N conversion. The conclusion we reach is that CN-strong stars reflect overabundances of N, driven mostly by O \rightarrow N conversion, but occasionally by C \rightarrow N conversion only. One might therefore expect that CN-strong stars would become more frequent members of the ensemble if O \rightarrow N and C \rightarrow N conversions plus deep-mixing were coupled to advancing evolutionary state (as seems to have happened in M13 (Kraft *et al.* 1997, Hanson *et al.* 1998)).

This idea does not work for M4. Defining an M4 star as “oxygen-depleted” if $[O/Fe] < +0.20$,¹⁴ eight of the eleven RGB stars are undepleted whereas three are significantly depleted in oxygen. Of these, six are CN-strong, one is CN-weak, and four have unknown CN strengths. Most RGB stars therefore show little depletion of oxygen, yet a number are CN-strong, which suggests that they are similar to L4201, in which carbon has been significantly transmuted to nitrogen. On the other hand, of the eleven AGB stars in our sample, nine suffer little or no oxygen depletion

¹⁴This choice of division between “depleted” and “undepleted” is meant to take into account the fact that the highest $[O/Fe]$ -ratios are typically near +0.40, and the typical observational error is ~ 0.10 dex. Changing the division point by 0.05 to 0.10 dex would not change the conclusions reached here in a significant way.

and all are classified as CN-weak. Only two are both oxygen-depleted and CN-strong. Thus the AGB population in M4 shows much less evidence for deep-mixing than does the RGB population, even though the AGB is a later stage of stellar evolution.

What explanation can be offered for this apparent anomaly? Since we have not so tacitly assumed that the CNO abundances observed reflect a “deep mixing” scenario, it is well to point out that this anomaly is not better explained by a “primordial” scenario in which one supposes that all CNO (and by implication Ne, Na, Mg and Al) abundances were completely imprinted in the original material out of which the present low-mass cluster stars were made. Rather it is the deep mixing scenario that may offer the most hope. Some time ago, Suntzeff (1981) showed that, in M3 and M13, the AGB is composed only of CN-poor stars which Suntzeff interpreted as evidence for significant mixing events prior to the evolution to the HB. In another study, Norris *et al.* (1981) noted that there are few CN-strong AGB stars in NGC 6752, as well as a gap in the HB of that cluster. They suggested that perhaps both effects not only had the same cause, but that the “...*high CN group does not ascend the giant branch for a second time*”. Later theoretical and observational work tends to support this idea. Langer & Hoffman (1995) proposed that deep mixing would alter the He/H ratio in the envelope of a red giant and send the descendant onto the blue part of the HB. The basic idea was extended and put on a firmer basis in calculations by Sweigart (1997a,b). A high-He star might fail to return to the AGB after occupation of the HB (e.g. HB evolutionary sequences of Dorman 1992). In the case of M13, virtually all giants near the red giant tip show evidence of very deep mixing (Kraft *et al.* 1997), and this in turn could be a major contributor not only to the “blueness” of M13’s HB but also to the relative paucity of AGB to RGB stars in that cluster (Caputo *et al.* 1978, Buzzoni *et al.* 1983).

Does this scenario apply in the case of M4? Caputo *et al.* (1978) proposed that M4 has a low ratio of AGB to RGB stars just like M13; however, Buzzoni *et al.* (1983) argued that the ratio is only slightly below average. Differential reddening across the face of M4 clouds the determination of this ratio and may account for the difference between the estimates. In addition, the depletion of O is much smaller in M4 than in M13, and, as we have asserted in §4.2.2, the enhancement of Al in M4 is compatible with the destruction of $^{25,26}\text{Mg}$ rather than the destruction of ^{24}Mg . Thus if deep mixing is required in M4 to explain the change in the abundances of C, N, O, Na, Mg and Al with evolutionary state, then the depth of mixing required is less than that presumed to occur in M13. The calculations of Langer & Hoffman (1995) indeed suggest that the H envelope depletion needed in M4 is less than 3%, whereas the requirement in the case of M13 appear to be closer to 15% (Kraft *et al.* 1998). Thus it is unclear if “mixed” M4 giants would ultimately evolve into HB stars that are too blue to return to the AGB. Smith and Norris (1993) observed seven RHB stars in M4 in a narrow $B-V$ range. Based on nitrogen-enhanced synthetic spectra modelling of the blue CN band, Smith & Norris find very little CN variation and, with cautionary words about the assumed $[\text{O}/\text{Fe}]$, $[\text{C}/\text{Fe}]$, and other uncertainties in the model-dependent result, suggest that the spectra of all seven stars might be analogs of the CN-strong red giants. It would be of interest to observe these same seven stars using a larger wavelength coverage, to

determine whether or not the stars still seem to be CN-strong in the red system, and to derive the abundances of the proton-capture nucleosynthesis elements, to determine whether the abundances of these much more evolved stars are consistent with our findings of the CN-strong/CN-weak abundance correlations among the giant branch stars. We emphasize once again that a purely primordial scenario would fare even worse in explaining the evolutionary abundance changes: only one of seven (relatively unevolved) RGB stars in our sample are designated as CN-weak.

5. Comparisons with Some Other Clusters

5.1. The Na *vs.* O Anticorrelation

5.1.1. M4 *vs.* M5

We first compare the Na *vs.* O anticorrelation of M4 with that of M5, a cluster having essentially the same metallicity as M4, and which was previously analyzed using techniques (Snedden *et al.* 1992) similar to those employed here. In Figure 16, we plot $[\text{Na}/\text{Fe}]$ *vs.* $[\text{O}/\text{Fe}]$ for the giants in these two clusters. Recall that we believe that, (a) L2208 is the one M4 giant in which the abundances of the α - and light odd elements are enhanced ab initio, and (b) L4201 is also the only M4 giant in which the CN-strong phenomenon is solely a result of C \rightarrow N conversion, O playing essentially no role. Eliminating these two stars (as well as the suspected binary L2406), we find that each cluster exhibits a noticeable Na *vs.* O anticorrelation, but the relationships are somewhat offset. The least “mixed” stars of M4 have higher O and higher Na abundances than those in M5 (by ~ 0.1 and ~ 0.2 dex, respectively), and the gap widens in the most mixed stars (to ~ 0.3 dex and ~ 0.25 dex, respectively). We note that, at comparable luminosities, M5 stars tend to have higher derived T_{eff} values than M4 stars. If there were an error in the temperature determinations for one cluster relative to another, could this generate the offsets illustrated in Figure 16? No, because from the T_{eff} dependencies listed in Table 6, a change in T_{eff} scales to force agreement between M4 and M5 would produce abundance changes having a direction opposite to that required. We therefore conclude that the offsets are probably real, and therefore that the ab initio O and Na abundances of M4 are a bit higher than those of M5. It has been amply demonstrated elsewhere (*e.g.* Pilachowski *et al.* 1996, Kraft *et al.* 1997) that there is a range of Na and O abundances among halo field giants which show little or no evidence of deep-mixing. It should, therefore, come as no surprise that the least mixed stars of globular clusters might exhibit variations in the abundances of these elements on the average from cluster to cluster.

A point of similarity exhibited in Figure 16 is that the *range* of the O and Na variations is about the same in the two clusters: for O, a factor of ~ 2.5 in M4 and a factor of ~ 3 in M5. Correspondingly, the Na factors are ~ 4.5 and ~ 4 , respectively. According to the deep mixing models of Langer & Hoffman (1995, their Fig. 1), a depletion of O by factors of 2.5 and 3 leads to enhancements of Na by factors of 4 and 5, respectively, in excellent agreement with what is

observed. The models assume, of course, that Ne, in addition to the other α -elements, is enhanced by 0.4 dex in $[\text{Ne}/\text{Fe}]$ above the solar value. We warn the reader that there is no way to determine spectroscopically if $[\text{Ne}/\text{Fe}] = +0.4$ or if the Ne abundance is the same in M4 as in M5, even if such assumptions are plausible. Since we argue that the ab initio O and Na might be slightly different in the two clusters, there is no assurance that Ne is not also slightly different.

In Figure 17, we exhibit the Na *vs.* O anticorrelation found in a number of intermediately metal-poor clusters having $[\text{Fe}/\text{H}]$ near -1.6 (see the figure caption for references). We omit M5, but superimpose the results from the present study of M4. Generally, we see that M4 is slightly offset from the other clusters: its ab initio Na and O abundances are a bit higher than in the other clusters, echoing its relationship to M5, although the differences are less extreme. The behavior of NGC 7006 seems closest to that of M4.

5.2. The Mg *vs.* Al Anticorrelation

In Figure 18, we plot $[\text{Al}/\text{Fe}]$ *vs.* $[\text{Na}/\text{Fe}]$ for our M4 sample as in Figure 15, but we now add M5 (Shetrone 1996a) and the two slightly more metal-poor clusters M13 (Kraft *et al.* 1997) and NGC 7006 (Kraft *et al.* 1998).

In M4, the range of variations of Al (~ 0.4 dex) and of Na (~ 0.6 dex) are internally consistent with the deep-mixing calculations of Langer & Hoffman (1995, their Fig. 1), which assume that the enhancements of Al and Na are generated at the expense of $^{25,26}\text{Mg}$ and ^{22}Ne , respectively. The NGC 7006 sample is quite small (six stars), but the range of both Al and Na is similar to that of M4, as is the “floor” of both $[\text{Na}/\text{Fe}]$ and $[\text{Al}/\text{Fe}]$. This suggests that the primordial sources of Al and Na (as well as their subsequent enhancements) in these two clusters may have a similar history. The distributions in M5 and M13 are, however, quite different from those of M4 and NGC 7006 where the abundance “floor” is clearly much lower for both $[\text{Na}/\text{Fe}]$ and $[\text{Al}/\text{Fe}]$ (~ -0.25 dex and ~ -0.1 dex, respectively). The range for M13 is very large and it has been argued elsewhere (Shetrone 1996a,b, Pilachowski *et al.* 1996, Kraft *et al.* 1998) that such a large range could only be induced if deep-mixing brought up the product of proton captures on ^{24}Mg . Although the ranges of Al and Na in M5 are much smaller than in M13, the current sample size in M5 is too small to claim that ^{24}Mg -depletion, as in M13, is ruled out. Clearly a larger sample of M5 giants is needed before a definitive picture can be established.

We plot $[\text{Al}/\text{Fe}]$ *vs.* $[\text{Mg}/\text{Fe}]$ in Figure 19, once again superimposing data from M5, M13, M15 and NGC 7006 from the references noted above. As in Figure 18, the range and location of the NGC 7006 data is similar to that of M4. In contrast to M4, M13 shows the large range of Al abundances compatible with destruction of ^{24}Mg (Shetrone 1996b). Striking, however, is the noticeable offset of Mg abundances in M5 with respect to M4, a reduction of Mg abundances by a factor of 2, on the average. Of the six M5 stars in the Shetrone sample, two are O-rich and four are O-poor (using the definition of §4.2.3); the CN classification is known for only two of these

(Smith *et al.* 1997, Smith & Norris 1983). Within the errors, the Mg abundances show little or no spread between the O-rich and O-poor subgroups. Once again, this suggests that among these stars, there has been little or no destruction of ^{24}Mg , independent of destruction of O. This in turn suggests that the *primordial abundance of Mg* (dominated by ^{24}Mg) *is higher in M4 than in M5*, despite the fact that the two clusters have virtually the same iron abundance. Again, this may not be surprising: among field halo giants (Pilachowski *et al.* 1996, Hanson *et al.* 1998), stars which exhibit no evidence for conversion of Ne to Na or Mg to Al, and therefore presumably reflect their original primordial abundances of these elements, the Mg and Na abundances are correlated. This indicates that there is a substantial primordial range in both of these elements at a given metallicity among halo field stars. Therefore it should come as no surprise that differences in the ab initio abundances of $[\text{Mg}/\text{Fe}]$ as well as $[\text{Na}/\text{Fe}]$ should exist from one cluster to another.

5.3. Alpha-Element Variations

To the evidence that Mg abundances in M4 exceed that in M5 by a factor of 2, we add the evidence that *silicon abundances in M4 also exceed that of M5 by a factor of 2*: $\langle[\text{Si}/\text{Fe}]\rangle_{M4} = +0.55 \pm 0.02$ (Table 5, 23 stars) *vs.* $\langle[\text{Si}/\text{Fe}]\rangle_{M5} = +0.20 \pm 0.02$ (Snedden *et al.* 1992; 13 stars). Ca and Ti abundances in the two clusters are essentially the same and have the “usual” modest overabundances (relative to Fe) in the +0.2 to +0.3 range. The α -elements of M4 are therefore somewhat unusual among clusters in the intermediately metal-poor range but mimic those found in the very metal-poor cluster M15 for which $[\text{Mg}/\text{Fe}] \sim +0.6$ (Snedden *et al.* 1997; for the 12 stars that have not experienced Mg depletion), $\langle[\text{Si}/\text{Fe}]\rangle = +0.60$ (12 stars), but $\langle[\text{Ca}/\text{Fe}]\rangle = +0.24$ (18 stars). In M15, $\langle[\text{Ti}/\text{Fe}]\rangle = +0.46 \pm 0.12$ but the result is not very reliable since it is based on only three stars. This Mg/Si “overabundance” *vs.* Ca/Ti “normal” abundance anomaly of M4 *vs.* M5, is seemingly accompanied by a correspondingly high “floor” of Al abundances, also found in M15. Substructure in α - and light odd elements is found also among relatively metal-rich ($[\text{Fe}/\text{H}] > -1$) disk dwarfs (*e.g.*, Edvardsson *et al.* 1993; *cf.*, Tomkin *et al.* 1997) and galactic nuclear bulge giants with metallicities near $[\text{Fe}/\text{H}] = -1$ (McWilliam & Rich 1994), but the distribution of the substructure does not always match that of either M4 or M5. For example, the galactic bulge giant BW IV-003 ($[\text{Fe}/\text{H}] = -0.94$) mimics the distribution of the α -elements and Al in M5, whereas BW IV-329 ($[\text{Fe}/\text{H}] = -0.85$) is similar to M4. However, there are other bulge giants in which these $[\text{el}/\text{Fe}]$ -ratios are dissimilar to both M4 and M5. And, in the disk dwarf sample of Edvardsson *et al.*, Ca and Si are paired as rising on the average more slowly with decreasing $[\text{Fe}/\text{H}]$ than Mg and Ti.

What does seem clear is that the differences between Mg, Si, Al and Na in M4 and M5 arise from some property of the primordial nucleosynthetic sites. Mg, Na and Al are the products of Ne- and C-burning. The α -elements are rather insensitive to the initial metallicity of the massive progenitor stars, but the abundances of both Na and Al are controlled by the neutron flux during the Ne- and C-burning. One expects $[\text{Al}/\text{Mg}] = C_1[\text{Mg}/\text{H}]$, and $[\text{Na}/\text{Mg}] = C_2[\text{Mg}/\text{H}]$, where

C_1 and C_2 are constants > 0 (Edvardsson *et al.* 1993). Considering the least “proton-capture enhanced” stars in both M4 and M5, we derive $C_1 = 0.15$ for M5 and 0.14 for M4. That is, the [Al/Fe] ratios for these two clusters are internally consistent if it is assumed that the Mg and Al abundances arise from a primordial nucleosynthetic site as described above. In the case of Na, we are less successful: on the same assumptions, we find $C_1 = 0.45$ for M5 but $C_2 = 1.00$ for M4. However, the least “enhanced” floor for Na is rather poorly known for M5, so the difference between the two values of C_2 may not be too significant.

5.4. Ba, La, and Eu Abundances in M4, M5 and ω Cen

Among halo field giants, and giants in clusters such as M71, M13 and M92, $\langle[\text{Eu}/\text{Fe}]\rangle$ ranges from +0.3 to +0.5 with little scatter within a given cluster (Shetrone 1996a). For M5, Shetrone found $\langle[\text{Eu}/\text{Fe}]\rangle = +0.44 \pm 0.03$, based on six stars. Thus the value we derive in the case of M4 (Table 5), $\langle[\text{Eu}/\text{Fe}]\rangle = +0.35 \pm 0.02$ is in no way unusual. What is surprising in M4 is the high abundance of Ba: $\langle[\text{Ba}/\text{Fe}]\rangle = +0.60 \pm 0.02$ (Table 5), which is supported by the high abundance of La: $\langle[\text{La}/\text{Fe}]\rangle = +0.45 \pm 0.02$. The [Ba/Eu] ratio, often taken as a measure of s - to r -process nucleosynthesis in the primordial material of the cluster, has the unusually high value of +0.25. Generally, field halo and globular cluster (M5, M13, M92) giants agree (Gratton & Sneden 1991, 1994, Armosky *et al.* 1994, Shetrone 1996a) that [Ba/Eu] is typically negative with a range from -0.2 to -0.6 . The [Ba/Eu] ratio in M4 is more than four times higher than that of the “normal” cluster M5, and is 0.25 dex higher than the total solar-system $r + s$ value.

We performed numerical experiments by combining our derived Ba, La, and Eu abundances using a solar-system r -process ratio among the elements (Cowan, 1999). We found that the s -process ratios of our individual stars agree fairly well to within the abundance errors and are enhanced over the solar ratios for these elements. The Ba abundance in M4 cannot be attributed to the r -process component; in the M4 stars, we have a larger $s:r$ -process contribution than in the sun. Furthermore, there is no dependence of [Ba/Fe] on evolutionary state in M4, *i.e.*, [Ba/Fe] on the AGB does not exceed [Ba/Fe] on the RGB. Therefore the Ba-excess cannot result from neutron captures on Fe-peak elements during a He shell flash episode on the AGB, but must be a signature of s -process enrichment of the primordial material out of which the low-mass M4 stars were formed. As emphasized by the referee, the presence, and especially the excess, of the s -process elements provides evidence that the period of star formation and mass-loss that preceded the formation of the observed stars in M4 was long enough for AGB stars to contribute their ejecta into the ISM of the cluster. This, in turn, implies that stars of intermediate mass, of 3–10 solar masses, had time to evolve. Contribution from the s -process is very well evidenced in the globular cluster ω Cen (Vanture *et al.*).

It is also the case that in the multimetallicity cluster ω Cen, there are many giants with Ba abundances that are ~ 0.6 dex higher than in clusters such as M5, M13 and M92 (Norris & Da Costa 1995b). At the same time, Smith *et al.* (1995) demonstrated that some ω Cen giants also

had unusually low [Eu/Fe]-ratios (between -0.2 and -0.7), so that the high [Ba/Eu] values were in some instances a result of a deficiency in Eu rather than an excess of Ba. Clearly ω Cen shares some abundance characteristics in common with M4 (there exists in ω Cen a subset of stars which have nearly identical elemental overabundances with respect to iron as seen in M4 for aluminum, silicon, barium, and lanthanum), but it also possesses a more complicated nucleosynthetic history than M4. The important point here is that the high Ba and La properties of M4 stars is surely a primordial, not an evolutionary, effect.

6. Summary

We have conducted a large-sample high and medium resolution spectroscopic survey of 35 giant stars in the nearby mildly metal-poor ($[\text{Fe}/\text{H}] = -1.18$) globular cluster M4. In studying M4, we were confronted with a cluster having interstellar extinction that is large and variable across the cluster face, and which may obey a non-standard extinction law. Therefore, we combined traditional spectroscopic analytical techniques with new approaches to temperature determinations in order to derive a self-consistent set of atmospheric parameters and abundances for our program stars. Using our spectroscopic results, we derive a total-to-selective extinction ratio of 3.4 ± 0.4 as well as an average $\langle E(B-V) \rangle$ reddening significantly lower than that estimated by using the dust maps made by Schlegel *et al.* (1998). Some caution should be used when using the dust maps to estimate reddening and extinction in regions of high extinction.

The derived abundances are summarized at the beginning of §4, and will not be repeated in detail here. We find evidence that silicon and aluminum are primordially overabundant by factors greatly exceeding (~ 2 to 3) the mild overabundances (relative to iron) usually seen in α - and light odd elements among halo field and globular cluster giants of comparable metallicity, such as M5 and M13. We also find that barium is overabundant by a factor of about 4, and show that the [Ba/Fe]-ratio is independent of evolutionary state among M4 giants, thus ruling out that the excess Ba is a result of nuclear processes occurring within the M4 giants themselves. These overabundances confirm the results of an earlier study (Brown & Wallerstein 1992) based on a much smaller sample of M4 giants.

Superimposed on the somewhat unusual primordial abundance distribution nevertheless is evidence for the existence of proton capture synthesis of carbon, oxygen, neon, and magnesium, which leads to the production of nitrogen from C and O, sodium from Ne and Al from Mg, probably as a result of deep-mixing of the stellar envelope through the hydrogen-burning shell. We recover the Na *vs.* O anticorrelation and Na *vs.* Al correlation found in other globular clusters. The the range of variation is muted as compared with more metal-poor clusters such as M13 and M15 but larger than that found in the more metal-rich cluster, M71. The rather small range of variation of Al in M4, plus the absence of any significant variation in Mg, is compatible with the idea that the Al enhancements are derived from the destruction of $^{25,26}\text{Mg}$, in contrast to the destruction of ^{24}Mg required in the case of M13. While the abundance swings of C, O, Na, Mg

and Al appear to be muted compared with what is seen in more metal-poor clusters, they have not entirely disappeared.

A puzzle arises from the fact that giants of the AGB have C,N,O abundances that show less evidence for proton capture nucleosynthesis than is found in the less-evolved stars of the RGB. We discuss the idea that deeply mixed stars of the RGB, subsequent to the He core flash, might take up residence on the blue end of the HB, and thus fail to evolve back to the AGB. Reasons for skepticism concerning this scenario are noted. On the other hand, attribution of this puzzle to a primordial scenario would fare even worse.

7. Acknowledgements

We are indebted to Jerry Lodriguss for generously sharing the electronic files containing his excellent deep sky images of the M4 Sco-Oph region. We also gratefully acknowledge Jeff Brown for supplying his EWs of three M4 stars; Tim Davidge and Flavio Fusi Pecci & Francesco Ferraro for sharing their photometry of M4; and Pamela Gay & David Lambert for notifying us of the results of their MgH work prior to publication as well as making their line lists available. David Schlegel has our appreciation for answering questions regarding the dust map code as does David Gray for providing helpful feedback regarding the applicability of the spectroscopic line ratio technique. We thank David Lambert, John Norris, Jim Truran, Neal Evans, John Lacy, Don Winget, Craig Wheeler, Jos Tomkin, and Vincent Woolf for helpful discussions and/or thoughtful comments on drafts of this paper. We also appreciate the valuable suggestions and remarks made by the referee, George Wallerstein, and the subsequent improvements that these also made to the paper, in particular, the recommendation to determine and analyze the La abundance in the context of the Ba enhancements.

IRAS fluxes were obtained using IBIS, an observational planning tool for the infrared sky developed at IPAC. The Infrared Processing and Analysis Center is operated by the California Institute of Technology and the Jet Propulsion Laboratory under contract to NASA. This project has also made use of NASA's Astrophysics Data System Abstract Service. This research was made possible by NSF grants AST-9217970 to RPK, AST-9618364 to CS, and AST-9618459 to VVS.

Ed Langer, our co-author, passed away on Feb. 16, 1999, following a brief illness. Ed's kindness and generous spirit added a great deal to our collaboration; his way of thinking about things clarified the basic physics at the heart of our observations and added a great deal to the science. He will be greatly missed.

REFERENCES

Alcaino, G. 1975, *A&AS*, 21, 5

- Arce, H. G. & Goodman, A. A. 1999a, ApJ, 512, L135
- Arce, H. G. & Goodman, A. A. 1999b, submitted to ApJ, astro-ph/9902110
- Armosky, B. J., Sneden, C., Langer, G. E., & Kraft, R. P. 1994, AJ, 108, 1364
- Barbuy, B. 1985, A&A, 151, 189
- Barlow, M. J. & Cohen, M. 1977 ApJ, 213, 737
- Briley, M. M. 1997, AJ, 114, 1051.
- Briley, M. M., Bell, R. A., Hesser, J. E., & Smith, G. H. 1994, Can. J. Phys., 72, 772
- Briley, M. M., Smith, V. V., Suntzeff, N. B., Bell, R. A., Hesser, J. E., Lambert, D. L., & Smith, G. H. 1999, preprint.
- Brown, J. A. 1998, private communication
- Brown, J. A. & Wallerstein, G. 1989, AJ, 98, 1643
- Brown, J. A., Wallerstein, G., & Oke, J. B. 1990, AJ, 100, 1561
- Brown, J. A. & Wallerstein, G. 1992, AJ, 104, 1818
- Buzzoni, A., Fusi Pecci, F., Buonanno, R., & Corsi, C. E. 1983, A&A, 128, 94
- Cacciari, C. 1983, ApJ, 268, 185
- Campbell, B. & Smith, G. H. 1987, ApJ, 323, L69
- Caputo, F., Castellani, V., & Wood, P. R. 1978, MNRAS, 184, 377
- Caputo, F., Castellani, V., & Quarta, M. L. 1985, A&A, 143, 8
- Cavallo, R. M., Sweigart, A. V., & Bell, R. A. 1998, ApJ, 492, 575.
- Chini, R. 1981, A&A, 99, 346
- Clayton, G. C. & Cardelli, J. A. 1988, AJ, 96, 695
- Cohen, J. G., Frogel, J. A., & Persson, S. E. 1978, ApJ, 222, 165
- Cottrell, P. L. & Da Costa, G. S. 1981, ApJ, 245, L79
- Cowan, J. J. 1999, private communication
- Cudworth, K. M. 1979, AJ, 84, 1866
- Cudworth, K. M. & Rees, R. F. 1990, AJ, 99, 1491
- de Bièvre, P. & Barnes, I. L. 1985, Internat. J. Mass. Spec. Ion Proc., 65, 211
- de Geus, E. J. & Burton, W. B. 1991, A&A, 246, 559
- Dickens, R. J., Croke, B. F. W., Cannon, R. D., & Bell, R. A. 1991, Nature, 351, 212
- Dixon, R. I. & Longmore, A. J. 1993, MNRAS, 265, 395
- Dorman, B. 1992, ApJS, 81, 221
- Drake, J. J., Smith, V. V., & Suntzeff, N. B. 1992, ApJ, 395, L95

- Drake, J. J., Smith, V. V., & Suntzeff, N. B. 1994, *ApJ*, 430, 610
- Dupree, A. K., Sasselov, D. D., & Lester, J. B. 1992, *ApJ*, 387, L85
- Edvardsson, B., Andersen, J., Gustafsson, B., Lambert, D. L., Nissen, P. E., & Tomkin, J. 1993, *A&A*, 275, 101
- Fitzpatrick, M. J. & Sneden, C. 1987, *BAAS*, 19, 1129
- Frogel, J., Persson, E., & Cohen, J. 1983, *ApJS*, 53, 713
- Fusi Pecci, F. & Ferraro, F. R. 1997, private communication
- Gay, P. L. & Lambert, D. L. 1999, private communication
- Gilroy, K. K. 1989, *ApJ*, 347, 835
- Gonzalez, G. & Wallerstein, G. 1998, *AJ*, in press
- Goodrich, R. W. & Veilleux, S. 1988, *PASP*, 100, 1572
- Gratton, R. G. 1987, *A&A*, 177, 177
- Gratton, R. G., Quarta, M. L., & Ortolani, S. 1986, *A&A*, 169, 208
- Gratton, R. G. & Sneden, C. 1991, *A&A*, 241, 501
- Gratton, R. G. & Sneden, C. 1994, *A&A*, 287, 927
- Gray, D. F. 1994, *PASP*, 106, 1248
- Gray, D. F. & Johanson, H. L. 1991, *PASP*, 102, 439
- Greenstein, J. L. 1939, *ApJ*, 90, 397
- Griffin, R. F. 1968, *A Photometric Atlas of the Spectrum of Arcturus $\lambda\lambda 3600\text{--}8825\text{\AA}$* , Cambridge Philosophical Society
- Gustafsson, B., Bell, R. A., Ericksson, K., & Nordlund, A. 1975, *A&A*, 42, 407
- Hanson, R. B., Sneden, C., Kraft, R. P., & Fulbright, J. 1998, *AJ*, 116, 1286
- Harris, D. H. 1973 in *Interstellar Dust and Related Topics*, IAU Symposium No. 52, ed. J. M. Greenberg & H. C. van de Hulst (Dordrecht: Reidel), p. 31
- Hiltgen, D. 1996, Ph.D. Thesis, University of Texas, Austin
- Iben, I. Jr. 1964, *ApJ*, 140, 1631
- Ingerson, T. E. 1993, in *Fibers Optics in Astronomy II*, ASP Conf. Ser., ed. P. M. Gray, 37, 76
- Kemp, S. N. & Bates, B. 1995, *A&AS*, 112, 513
- Kraft, R. P. 1994, *PASP*, 106, 553
- Kraft, R. P., Sneden, C., Langer, G. E., & Prosser, C. F. 1992, *AJ*, 104, 645
- Kraft, R. P., Sneden, C., Langer, G. E., & Shetrone, M. D. 1993, *AJ*, 106, 1490
- Kraft, R. P., Sneden, C., Langer, G. E., Shetrone, M. D., & Bolte, M. 1995, *AJ*, 109, 2586

- Kraft, R. P., Sneden, C., Smith, G. H., Shetrone, M. D., Langer, G. E., & Pilachowski, C. A. 1997, *AJ*, 113, 279
- Kraft, R. P., Sneden, C., Smith, G. H., Shetrone, M. D. & Fulbright, J. 1998, *AJ*, 115, 1500
- Kurucz, R. L. 1993 in Peculiar versus Normal Phenomena in A-type and Related Stars, ASP Conf. Ser., ed. M. M. Dworetsky, F. Castelli, & R. Faraggiana, 44, 87
- Lambert, D. L. & McWilliam, A. 1986, *ApJ*, 304, 436
- Lambert, D. L., McWilliam, A. & Smith, V. V. 1992 *ApJ*, 386, 685
- Lambert, D. L., Heath, J. E., Lemke, M., & Drake, J. 1996, *ApJS*, 103, 183
- Langer, G. E., Fisher, D., Sneden, C., & Bolte, M. 1998, *AJ*, 115, 685
- Langer, G. E. & Hoffman, R. 1995, *PASP*, 107, 1177
- Langer, G. E., Hoffman, R., & Sneden, C. 1993, *PASP*, 105, 301
- Langer, G. E., Hoffman, R., & Zaidins, C. S. 1997, *PASP*, 109, 244
- Langer, G. E., Bolte, M., & Sandquist, E. 1998, *ApJ*, submitted.
- Lee, S.-W. 1977, *A&AS*, 27, 367
- Liu, T. & Janes, K. A. 1990, *ApJ*, 360, 561
- Lloyd Evans, T. 1977, *MNRAS*, 178, 353
- Lyons, M. A., Bates, B., Kemp, S. N., & Davies, R. D. 1995, *MNRAS*, 277, 113
- McWilliam, A. & Rich, R. M. 1994, *ApJS*, 91, 749
- McWilliam, A., Preston, G. W., Sneden, C., & Searle, L. 1995, *AJ*, 109, 2757
- Moore, C. E., Minnaert, M. G. J., & Houtgast, J. 1966 *The Solar Spectrum 2935Å to 8770Å*, NBS Mono. 61, (Washington: U.S. Gov. Printing Off.)
- Norris, J. 1981, *ApJ*, 248, 177
- Norris, J. & Bessell, M. S. 1978, *ApJ*, 225, L49
- Norris, J., Cottrell, P. L., Freeman, K. C., & Da Costa, G. S. 1981, *ApJ*, 244, 105
- Norris, J. E. & Da Costa, G. S. 1995a, *ApJ*, 441, L81
- Norris, J. E. & Da Costa, G. S. 1995b, *ApJ*, 447, 680
- Norris, J. E., Freeman, K. C., & Mighell, K. J. 1996, *ApJ*, 462, 241
- Paltoglou, G. & Norris, J. E. 1989, *ApJ*, 336, 185
- Peterson, R. C., Rees, R. F., & Cudworth, K. M. 1995 *ApJ*, 443, 124
- Pilachowski, C. A., Sneden, C., & Kraft, R. P., 1996, *AJ*, 111, 1689
- Rood, R. T. 1972, *ApJ*, 177, 681.
- Schlegel, D. J., Finkbeiner, D. P., & Davis, M. 1998, *ApJ*, 500, 525

- Sawyer Hogg, H. 1973, Publ. David Dunlap Obs, 3, No. 6
- Schultz, G. V. & Wiemar, W. 1975 A&AS, 43, 133
- Shetrone, M. D. 1996a, AJ, 112, 1517
- Shetrone, M. D. 1996b, AJ, 112, 2639
- Shetrone, M. D. 1999, BAAS, 30, 1345.
- Simoda, M. & Tanikawa, K. 1970, PASJ, 22, 143
- Smith, G. H. & Norris, J. E. 1982, ApJ, 254, 149
- Smith, G. H. & Dopita, M. A. 1983, ApJ, 271, 113
- Smith, G. H. 1984, AJ, 89, 801
- Smith, G. H. & Wirth, G. D. 1991, PASP, 103, 1158
- Smith, G. H. & Norris, J. E. 1993, AJ, 105, 173
- Smith, G. H., Shetrone, M. D., Briley, M. M., Churchill, C. W., & Bell, R. A. 1997, PASP, 109, 236.
- Smith, V. V. & Suntzeff, N. B. 1989, AJ, 97, 1699
- Snedden, C. 1973, ApJ, 184, 839
- Snedden, C., Gehrz, R. H., Hackwell, J. A., York, D. G., & Snow, T. P. 1978, ApJ, 223, 168
- Snedden, C., Kraft, R. P., Prosser, C. F., & Langer, G. E. 1991, AJ, 102, 2001
- Snedden, C., Kraft, R. P., Prosser, C. F., & Langer, G. E. 1992, AJ, 104, 2121
- Snedden, C., Kraft, R. P., Langer, G. E., Prosser, C. F., & Shetrone, M. D. 1994, AJ, 107, 1773
- Snedden, C., Kraft, R. P., Shetrone, M. D., Smith, G. H., Langer, G. E., & Prosser, C. F. 1997, AJ, 114, 1964
- Suntzeff, N. B. 1981, ApJS, 47, 1
- Suntzeff, N. B. 1993, in The Globular Cluster-Galaxy Connection, ASP Conf. Ser., ed. G. H. Smith & J. B. Brodie, 48, 167
- Suntzeff, N. B, Mateo, M., Terndrup, D., Olszewski, E. W, Geisler, D., Weller, W. 1993, ApJ, 418, 208
- Suntzeff, N. & Smith, V. 1991, ApJ, 381, 160
- Sweigart, A. V. 1997, ApJ, 474, L23
- Sweigart, A. V. 1997, “Third Conference on Faint Blue Stars”, ed. A. G. D. Philip, J. W. Liebert, & R. A. Safford (Schenectady: L. Davis Press), p. 3
- Sweigart, A. V. & Gross, P. G. 1978, ApJS, 36, 405.
- Sweigart, A. V. & Mengel, J. G. 1979, ApJ, 229, 624
- Thévenin, F. 1990, A&AS, 82, 179

- Tomkin, J. & Lambert, D. L. 1980, *ApJ*, 235, 925
- Tomkin, J., Edvardsson, B., Lambert, D. L., & Gustafsson, B. 1997, *A&A*, 327, 587
- Tull, R. G., MacQueen, P. J., Sneden, C., & Lambert, D. L. 1995, *PASP*, 107, 251
- Twarog, B. J., Twarog, B. A., & Craig, J. 1995, *PASP*, 107, 32
- Valenti, J. A., Butler, R. P., & Marcy, G. W. 1995, *PASP*, 107, 966
- Vogt, S. S. 1987, *PASP*, 99, 1214
- Vrba, F. J., Coyne S.J., G. V., & Tapia, S. 1993, *AJ*, 105, 1010.
- Wallerstein, G, Iben, I. Jr., Parker, P., Boesgaard, A. M., Hale, G. M., Champagne, A. E., Barnes, C. A., Käppeler, F., Smith, V. V., Hoffman, R. D., Timmes, F. X., Sneden, C., Boyd, R. N., Meyer, B. S., & Lambert, D. L. 1997, *Rev. Mod. Phys.*, 69, 995
- Wallerstein, G., Leep, E. M., & Oke, J. B. 1987, *AJ*, 93, 1137
- Whitmer, J. C., Beck-Winchatz, B., Brown, J. A., & Wallerstein, G. 1995, *PASP*, 107, 127
- Worthey, G. 1994, private communication
- Woudt, P. A. 1998, Ph.D. Thesis, University of Cape Town, South Africa.
- Zinn, R. & West, M. J. 1984, *ApJS*, 55, 45

Figure Captions

Fig. 1.— A color-magnitude diagram of M4, with photometry from Cudworth & Rees (1990), showing the positions of our program stars on the giant branch. The symbols are given in the figure legend and correspond to the observatory and resolution of the spectrograph used for each observation. The inset diagram shows the program stars plotted in relation to all Cudworth & Rees M4 stars of magnitude ≤ 15.5 .

Fig. 2.— A reduced, “raw”, normalized spectrum of M4 L3413 in the region near the important $\lambda 6300.3 \text{ \AA}$ O I line, a “telluric standard” hot, rapidly rotating divisor star (in this case ζ Oph), and the “final” quotient spectrum, essentially free of telluric lines. The relative flux scale of the L3413 is correct, and the other spectra have been shifted vertically by additive constants for display.

Fig. 3.— High resolution 2d-coudé and medium resolution Argus spectra surrounding the $\lambda 6300.3 \text{ \AA}$ [O I] line in M4 stars L1514 (an RGB tip star) and L2206 (a star near the low-luminosity limit of the high resolution data). The relative flux scale of the L1514 high resolution spectrum is correct, and the other spectra have been shifted vertically by additive constants for display. The O I line and several temperature-sensitive Ti I and V I lines are marked in the figure. Most of the remaining prominent absorption features are due to Fe I.

Fig. 4.— Spectroscopic lines whose ratios are good T_{eff} indicators: M4 stars L1701 (4625K) and L1411 (3950K) are shown, with a vertical offset added to the L1701 spectrum. Lines that are temperature-variable according to Gray (1994) are indicated with “V” labels, and those that are temperature-stable are marked with “S” labels.

Fig. 5.— Two typical line-depth ratios plotted as functions of T_{eff} in M4 and three comparison clusters observed in earlier papers of this series (a comprehensive investigation of the spectroscopic line ratios of these data sets is underway and will be reported in a future publication). The ratios are presented in logarithmic form, and the dividend and divisor lines are labeled both by Gray’s (1994) numbering scheme (*e.g.*, d5, d6) and by atomic species. The scatter in the relationships with respect to T_{eff} increases at higher temperatures because the line depths (especially those of the dividend lines) become weak just as the typical S/N of the spectra are becoming less in these fainter stars.

Fig. 6.— A map of M4, showing the positions of the program stars we observed at high resolution using the Lee (1977) stellar identification scheme. The relative stellar position information in seconds of arc is taken from Cudworth & Rees (1990). Our 2d-coudé observations are denoted by shaded circles. The remaining stars are denoted by hollow squares (where the size of the square roughly indicates a star’s relative magnitude). We also show our derived $E(B - V)$ estimates.

Fig. 7.— A boxplot of the M4 giant star element abundances. A boxed horizontal line indicates the

interquartile range (the middle 50% of the data) and median found for a particular element. The vertical tails extending from the boxes indicate the total range of abundances determined for each element, excluding outliers. Mild outliers (those between $1.5\times$ and $3\times$ the interquartile range) are denoted by hollow circles (o) and severe outliers (those greater than $3\times$ the interquartile range) by filled circles (\bullet). The dashed line at $[\text{el}/\text{Fe}]$ represents the solar value for a particular elemental abundance ratio.

Fig. 8.— Abundances of the Fe-peak and neutron-capture elements (Sc, Ti, V, Ni, Ba, La, and Eu) with respect to the iron abundance as functions of effective temperature. A dashed line at $[\text{el}/\text{Fe}] = 0.0$ represents the solar value for a particular elemental abundance. CN-weak stars are denoted by open circle symbols (o) and CN-strong stars are denoted by filled circles (\bullet). Hollow squares (\square) denote the values derived for the three program stars cooler than 3900 K, for which our abundances are not considered to be as reliable.

Fig. 9.— Carbon abundances derived by SS91 plotted versus their T_{eff} values. For the stars observed in our study, denoted by filled circles (\bullet), we indicate with arrows the adjusted C abundances for the indicated higher T_{eff} 's of this work.

Fig. 10.— Representative spectra of the CN (2–0) bandhead region at 7874 \AA of four of our M4 stars and a “telluric standard” star, ζ Oph. The spectra between the two vertical dashed lines illustrate the region we used to measure EW. The stars presented are listed in the following order, from top to bottom: L4511, a star which appears to be very CN-strong in both the red and the blue measures; L3413, a star of similar T_{eff} but of very weak CN-strength (as measured in the red); L4414 and L4633, a warmer pair of stars, showing a similar contrast in CN-strength at a higher T_{eff} .

Fig. 11.— A comparison of the S(3839) index from Norris (1981) or SS91 (or a mean for the stars in common) and our EW7874 measure, plotted as a function of the observed magnitude. The solid circles (\bullet) in the upper plot are those stars in common with this study. The lower plot includes all of the stars observed at high resolution used in this study. The baseline for the S(3839) plot is from Norris and the V magnitudes are taken from Cudworth & Rees (1990) for stars observed in this study with the remainder taken from Lee (1977).

Fig. 12.— An H-R diagram for the M4 giant stars of the present survey. The symbols are explained in the figure legend, and derivation of the M_{bol} values are explained in the text (§4.1). The regions encompassing the RGB and AGB stars (discussed in §4.2.3) are marked on the figure. We note two stars with wavelength-dependent CN-designations.

Fig. 13.— Carbon abundances (from SS91, adjusted to our stellar parameters), nitrogen abundances (determined by syntheses of the CN (2–0) bands near $\lambda 8005 \text{ \AA}$), and C+N+O total abundance plotted versus O abundances (determined by syntheses of the $\lambda\lambda 6300, 6363 \text{ \AA}$ forbidden

oxygen lines). CN-strong and CN-weak stars are denoted and the CN strengths appear to correlate with the oxygen abundances. As earlier, hollow squares (\square) denote values derived for any of the the three program stars cooler than 3900 K, for which our abundances are less reliable.

Fig. 14.— Sodium abundances (determined by syntheses of the Na lines at $\lambda\lambda 5682$ and 5688 \AA) and aluminum abundances (determined by equivalent width analysis of the doublets at $\sim \lambda\lambda 6696, 7836, 8773 \text{ \AA}$) plotted versus oxygen abundances. CN-strong and CN-weak stars are denoted and the CN strengths appear to correlate with the abundances. Note that the ordinate and abscissa are plotted to different scales. Two stars stand out and are discussed in the text (§4.2.2).

Fig. 15.— Sodium abundances and magnesium abundances (the latter determined by the synthesis of $\lambda 5711 \text{ \AA}$ Mg I and the equivalent width analyses of $\lambda\lambda 5528, 7692 \text{ \AA}$) plotted versus the aluminum abundances. CN-strong and CN-weak stars are denoted and the CN strengths appear to correlate with the Al abundances.

Fig. 16.— Sodium abundances plotted versus oxygen abundances for M4 and M5 (where the scale is the same as that of Figure 17). Two stars stand out and are discussed in the text (§4.2.2 and 5.1.1.).

Fig. 17.— Sodium abundances plotted versus oxygen abundances for M4 and other slightly lower-metallicity clusters.

Fig. 18.— Aluminum abundances plotted versus sodium abundances for M4, M5, and other slightly lower-metallicity clusters.

Fig. 19.— Aluminum abundances plotted versus magnesium abundances for M4 as well as previous high resolution abundance studies of other clusters of a range of metallicities. In M4, the abundances appear to be uncorrelated whereas other clusters show both correlated and anticorrelated Mg-Al behavior. However, as illustrated in the figure, the fit between the results we obtained for M4 and those of other clusters is gratifying.

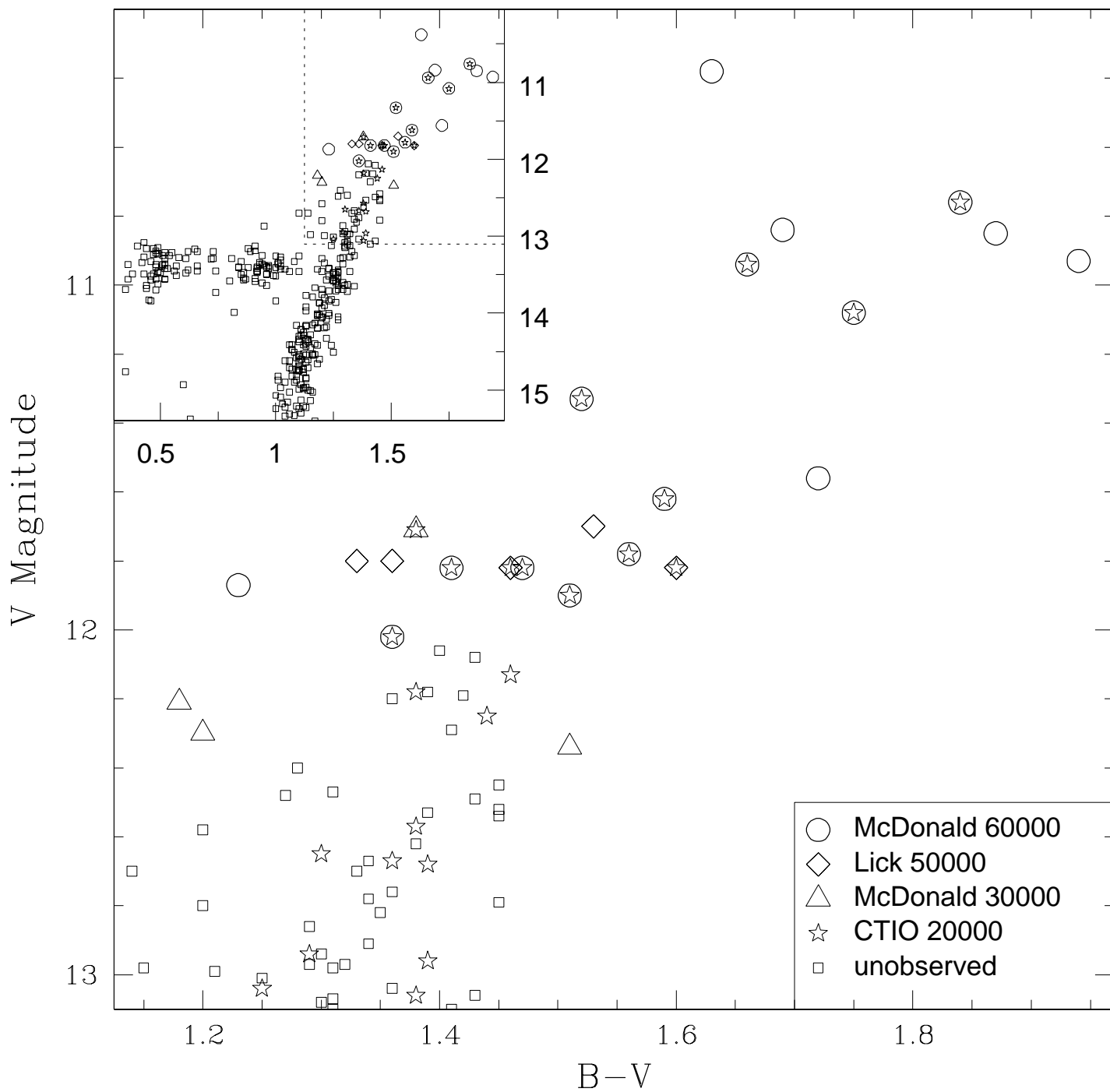


TABLE 1. M4 Observational Data

Star ^(a)	Alt.	V ^(b)	B-V ^(b)	Date (UT)	Instrument	R	Exp. (min)	S/N	v_r ^(c) (km/s)	v_r ^(d) (km/s)	σ ^(d) (km/s)
L1412	V4, ALX	10.38	1.63	1997 Mar 28	2d-coudé	60,000	30	115	+67.55	+70.76	0.42
				1998 Feb 08	2d-coudé	30,000	30	170	+67.55	+61.29	0.91
L1514	...	10.76	1.84	1997 Mar 27	2d-coudé	60,000	45	95	+78.27	+79.47	0.42
				1992 Sep 18	Argus	20,000	95	85	+78.27	+79.15	0.13
L2406	V13	10.84	1.69	1997 Apr 12	2d-coudé	60,000	50	90	+69.58	+71.16	0.37
L4613	A516	10.85	1.87	1997 Mar 28	2d-coudé	60,000	45	65	+68.61	+68.75	0.41
L4611	A515	10.93	1.94	1997 Mar 28	2d-coudé	60,000	45	75	+65.08	+64.84	0.45
L3209	...	10.94	1.66	1997 Apr 13	2d-coudé	60,000	45	85	+66.26	+64.70	0.53
				1992 Sep 18	Argus	20,000	95	60	+66.26	+65.54	0.22
L1411	A219	11.08	1.75	1997 Apr 14	2d-coudé	60,000	100	85	+69.01	+68.61	0.59
				1992 Sep 18	Argus	20,000	95	80	+69.01	+69.03	0.16
L3413	A95	11.33	1.52	1997 Apr 15	2d-coudé	60,000	100	125	+67.16	+66.77	0.43
				1992 Sep 18	Argus	20,000	95	65	+67.16	+67.53	0.21
L2307	...	11.56	1.72	1997 Apr 23	2d-coudé	60,000	45	75	...	+69.15	0.41
L4511	...	11.62	1.59	1997 Apr 16	2d-coudé	60,000	100	65	+66.12	+65.73	0.41
				1992 Sep 18	Argus	20,000	95	55	+66.12	+66.38	0.38
L1501	A243	11.70	1.53	1997 Jun 30	Hamilton	50,000	60	70	+69.90	+70.72	0.73
L4201	...	11.71	1.38	1997 Jun 18	2d-coudé	30,000	30	125	+75.42	+76.62	0.45
				1992 Sep 18	Argus	20,000	95	70	+75.42	+74.42	0.10
L3624	A459	11.78	1.56	1997 Apr 12	2d-coudé	60,000	95	100	+70.22	+69.44	0.44
				1992 Sep 18	Argus	20,000	95	60	+70.22	+69.29	0.30
L4633	A489	11.80	1.36	1997 Jul 01	Hamilton	50,000	60	55	...	+73.45	0.53
L4414	A142	11.80	1.33	1997 Jul 01	Hamilton	50,000	60	40	+65.95	+65.48	0.41
L2617	A529	11.82	1.60	1997 Jul 01	Hamilton	50,000	60	50	+63.62	+64.30	0.73
				1992 Sep 18	Argus	20,000	95	50	+63.62	+64.73	0.10
L3612	A468	11.82	1.47	1997 Apr 13	2d-coudé	60,000	80	70	+74.90	+72.46	0.44
				1992 Sep 18	Argus	20,000	95	75	+74.90	+74.84	0.44
L2519	A423	11.82	1.46	1997 Jun 30	Hamilton	50,000	60	75	+66.65	+67.08	0.57
				1992 Sep 18	Argus	20,000	95	95	+66.65	+66.23	0.10
L1408	B	11.82	1.41	1997 Mar 27	2d-coudé	60,000	90	115	+74.67	+73.37	0.37
				1992 Sep 18	Argus	20,000	95	105	+74.67	+73.37	0.28
L3207	...	11.87	1.23	1997 Apr 13	2d-coudé	60,000	80	105	+73.20	+73.39	0.32
L2206	...	11.90	1.51	1997 Apr 15	2d-coudé	60,000	100	80	+70.48	+69.93	0.45
				1992 Sep 18	Argus	20,000	95	80	+70.48	+69.94	0.25
L1701	A523	12.02	1.36	1997 Apr 16	2d-coudé	60,000	50	40	+72.71	+73.04	0.50
				1997 Apr 22	2d-coudé	60,000	90	115	+72.71	+73.00	0.54
				1992 Sep 18	Argus	20,000	95	95	+72.71	+73.15	0.11
L1403	C	12.13	1.46	1992 Sep 18	Argus	20,000	95	80	+72.76	+72.14	0.34
L1617	A399	12.18	1.38	1992 Sep 18	Argus	20,000	95	80	+67.96	+68.72	0.41
L3215	...	12.21	1.18	1997 Jun 17	2d-coudé	30,000	60	80	...	+66.59	0.52
L2608	A442	12.25	1.44	1992 Sep 18	Argus	20,000	95	55	+77.29	+78.11	0.97
L2208	D	12.30	1.51	1998 Feb 08	2d-coudé	30,000	70	85	+76.70	+76.34	0.50
L4302	A166	12.30	1.20	1997 Jun 18	2d-coudé	30,000	30	60	...	+67.86	0.56
L4513	...	12.49	1.14	1997 Jun 18	2d-coudé	30,000	30	45	-46.78	-45.79	0.50
L4415	A140	12.57	1.38	1992 Sep 18	Argus	20,000	95	95	+74.87	+75.93	0.33
L4413	A131	12.65	1.30	1992 Sep 18	Argus	20,000	95	85	+68.40	+68.86	0.49
L4421	...	12.67	1.36	1992 Sep 18	Argus	20,000	95	75	+67.65	+67.94	0.49
L2410	A284	12.68	1.39	1992 Sep 18	Argus	20,000	95	75	+66.14	+66.87	0.49
L4105	...	12.94	1.29	1992 Sep 18	Argus	20,000	95	85	+69.16	+67.76	0.78
G273	...	12.96	1.39	1992 Sep 18	Argus	20,000	95	70	+67.06	+66.74	0.46
L4206	A119	13.04	1.25	1992 Sep 18	Argus	20,000	95	45	+66.63	+65.62	0.41
L2305	A54	13.06	1.38	1992 Sep 18	Argus	20,000	95	65	+74.03	+73.09	0.51

^(a)Stellar identifications adopted from Lee (1977).

^(b) V and $B - V$ taken from Cudworth & Rees (1990).

^(c)Radial velocity information taken from Peterson, Rees, and Cudworth (1995).

^(d)Radial velocity information determined in this study.

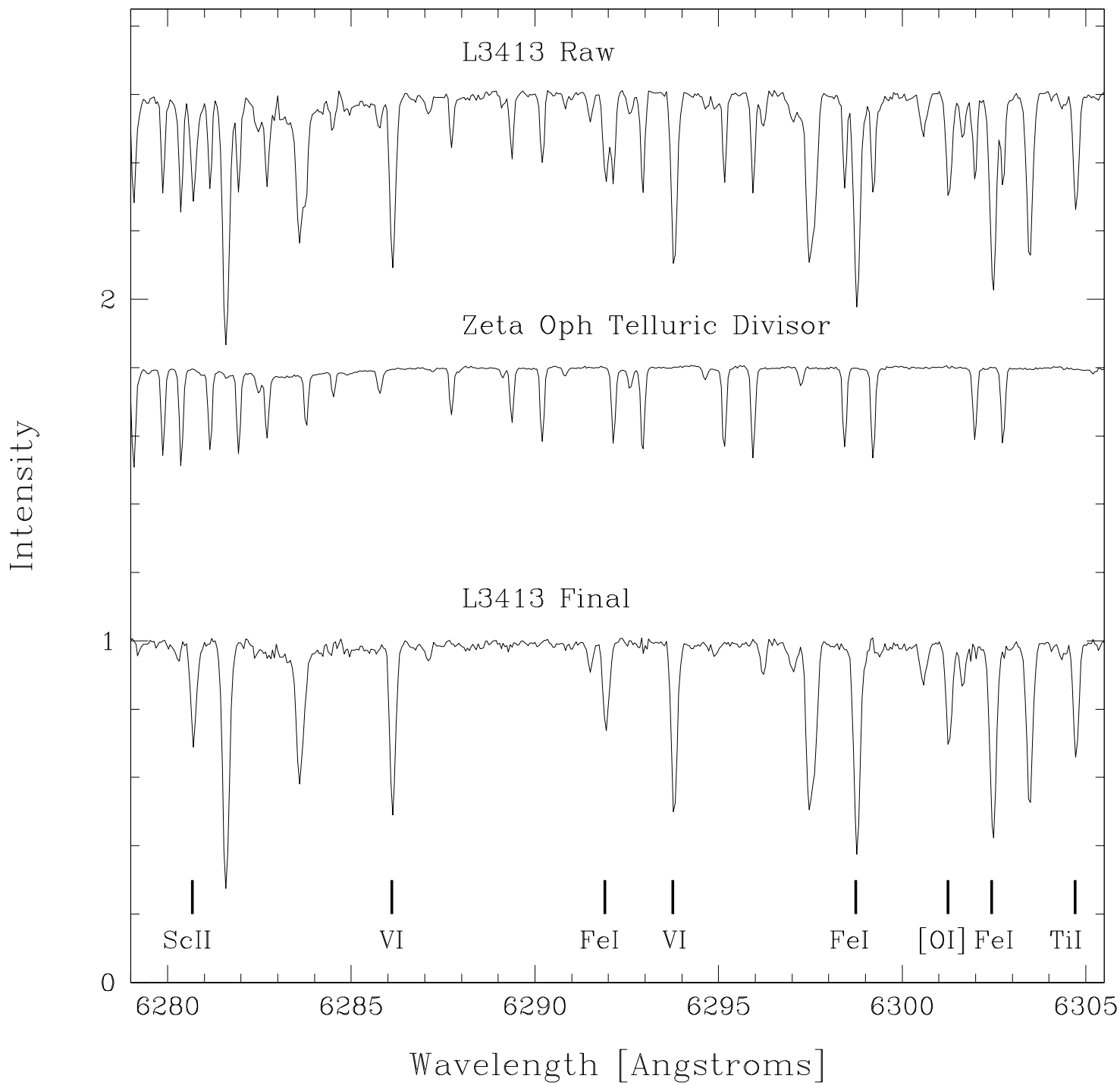


TABLE 2. Final Model Parameters

Star	(B-V)	(B-V) _c ^a	T _{eff}	log g spec	log g evol	δ(log g) ^b	v _t km s ⁻¹	[Fe/H] Fe I	[Fe/H] Fe II	[Ti/Fe] ^c Ti I	[Ti/Fe] ^c Ti II
L4611	1.94	1.94	3725	+0.30	+0.25	+0.05	1.70	-1.16	-1.17	+0.28	+0.31
L4613	1.87	1.87	3750	+0.20	+0.25	-0.05	1.65	-1.19	-1.15	+0.34	+0.30
L1514	1.84	1.83	3875	+0.35	+0.32	+0.03	1.95	-1.23	-1.08	+0.34	+0.23
L1411	1.75	1.73	3950	+0.60	+0.52	+0.08	1.65	-1.21	-1.18	+0.39	+0.38
L3209	1.66	1.69	3975	+0.60	+0.57	+0.03	1.75	-1.22	-1.18	+0.37	+0.31
L2307	1.72	1.70	4075	+0.85	+0.84	+0.01	1.45	-1.20	-1.17	+0.36	+0.31
L2406	1.69	1.69	4100	+0.45	+0.58	-0.13	2.45	-1.22	-1.18	+0.25	+0.24
L4511	1.59	1.61	4150	+1.10	+0.98	+0.12	1.55	-1.16	-1.21	+0.37	+0.37
L1501	1.53	1.51	4150	+0.85	+0.95	-0.10	1.50	-1.20	-1.20	+0.37	+0.41
L3413	1.52	1.55	4175	+1.20	+0.90	+0.30	1.65	-1.18	-1.15	+0.30	+0.24
L2617	1.60	1.59	4200	+0.95	+1.06	-0.11	1.55	-1.18	-1.16	+0.28	+0.31
L3624	1.56	1.56	4225	+1.10	+1.09	+0.01	1.45	-1.16	-1.15	+0.33	+0.32
L3612	1.47	1.48	4250	+1.10	+1.13	-0.03	1.45	-1.20	-1.17	+0.34	+0.36
L2206	1.51	1.48	4325	+1.35	+1.15	+0.20	1.55	-1.18	-1.18	+0.35	+0.34
L2208	1.51	1.46	4350	+1.40	+1.34	+0.06	1.70	-1.12	-1.22	+0.34	+0.40
L2519	1.46	1.44	4400	+1.20	+1.20	0.00	1.85	-1.18	-1.14	+0.29	+0.21
L4201	1.38	1.41	4450	+1.35	+1.22	+0.13	1.85	-1.19	-1.17	+0.22	+0.16
L4633	1.36	1.37	4500	+1.15	+1.30	-0.15	1.65	-1.17	-1.21	+0.30	+0.33
L1408	1.41	1.39	4525	+1.30	+1.27	+0.03	1.70	-1.18	-1.23	+0.27	+0.29
L4414	1.33	1.35	4525	+1.25	+1.33	-0.08	2.00	-1.14	-1.17	+0.27	+0.32
L1701	1.36	1.35	4625	+1.50	+1.44	+0.06	1.65	-1.20	-1.20	+0.25	+0.26
L3207	1.23	1.27	4700	+1.65	+1.49	+0.16	1.70	-1.18	-1.15	+0.23	+0.23
L3215	1.18	1.21	4775	+1.40	+1.59	-0.19	1.85	-1.17	-1.23	+0.32	...
L4302	1.20	1.20	4775	+1.45	+1.62	-0.17	1.80	-1.18	-1.21	+0.18	+0.20

^a(B-V)_c is the observed (B-V) corrected only for differential reddening across the face of the M4, following the formula derived by Cudworth & Rees (1990).

^bδ(log g) ≡ log g_{spec} - log g_{evol}

^c[Ti/Fe] is with respect to the mean of the [Fe/H] values.

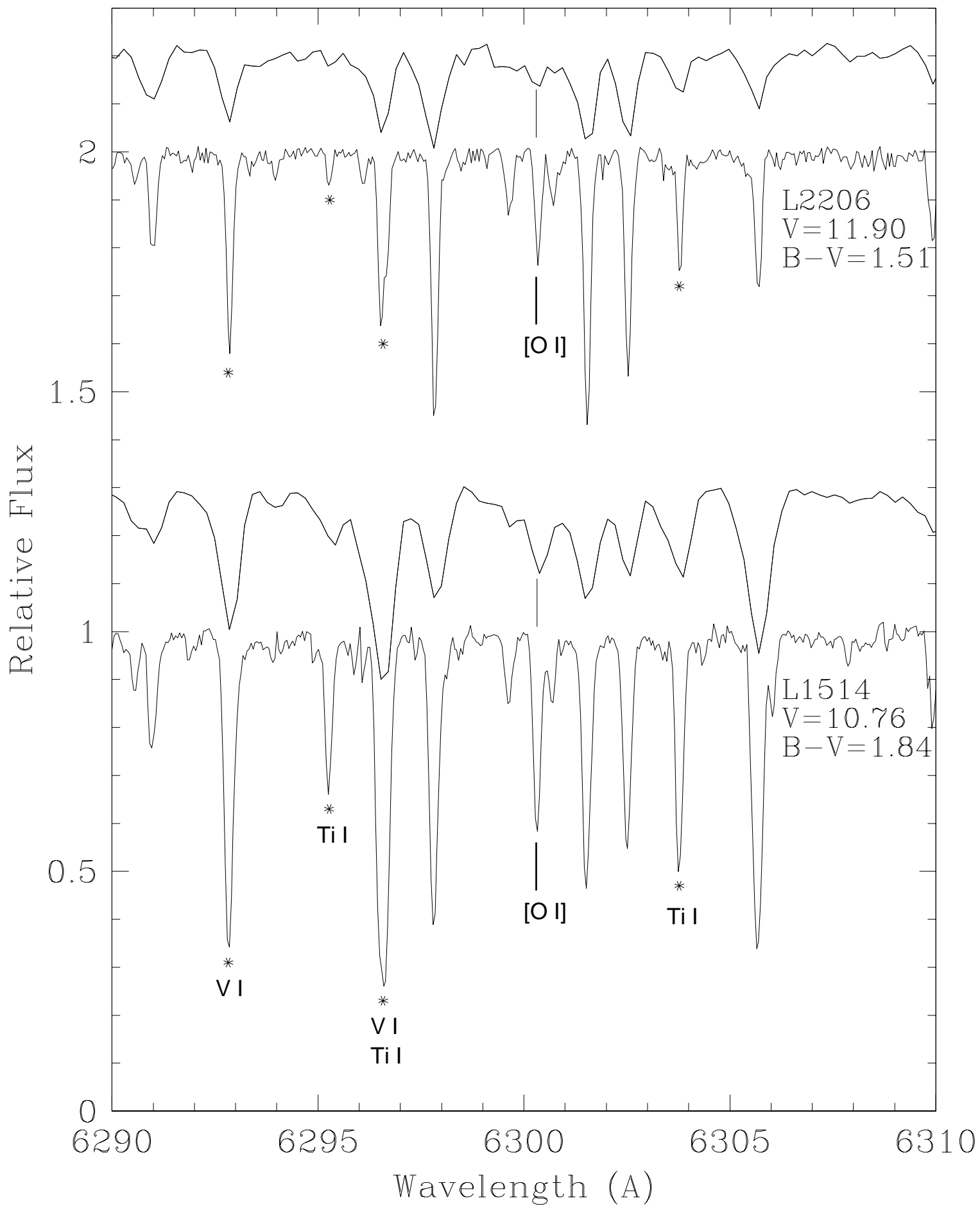


TABLE 3. H- α Emission Comparisons with Other M4 Work

Star	1997 ^a	1992 ^b	1990 ^c	1979 ^d
L4611	red	both	blue:	blue
L4613	blue	blue	blue	blue:
L1514	...	blue:	...	none
L1411	...	none
L3209	...	blue	blue:	...
L2307	...	none
L2406	...	both
L1501	none
L3413	...	none
L2617	red:
L3624	...	none
L2206	...	none
L2519	none
L4201	...	none
L4633	none	none
L4414	none	none
L3207	...	none
L3215	...	none
L1412	...	both	both	...

^aThis study

^bKemp & Bates (1995)

^cBrown *et al.* (1992)

^dCacciari & Freeman (1983)

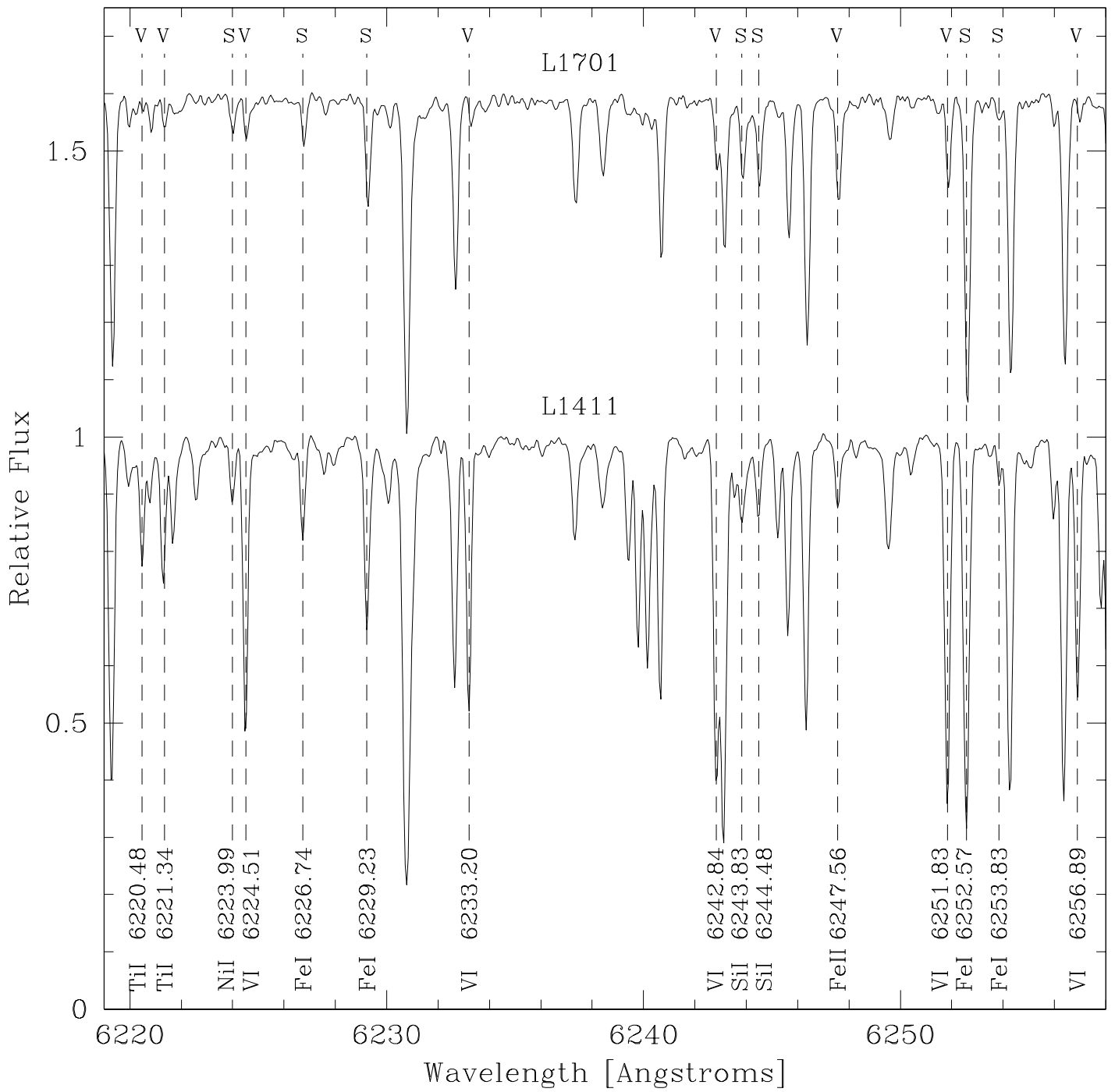


TABLE 4. Reddening Comparisons with Other M4 Work

Star	E(B-V) spec ^a	E(B-V) K I ^b	$\delta E(B-V)^c$	IRAS (mJy) ^d
Values for Individual Stars				
L4611	...	0.41	...	103.2
L4613	...	0.36	...	103.2
L1514	0.29	0.32	-0.03	103.2
L1411	0.31	0.29	+0.02	101.3
L3209	0.25	0.26	-0.01	95.2
L2307	0.40	0.30	+0.07	110.2
L2406	0.39	0.32	+0.07	105.2
L4511	0.33	100.2
L1501	0.27	100.2
L3413	0.28	0.29	-0.01	95.2
L2617	0.38	102.2
L3624	0.36	0.39	-0.03	103.2
L3612	0.29	101.2
L2206	0.37	0.26	+0.11	107.2
L2208	0.39	114.2
L2519	0.36	100.2
L4201	0.30	0.33	-0.03	100.3
L4633	0.31	0.36	-0.05	101.2
L1408	0.37	101.2
L4414	0.29	0.35	-0.06	100.2
L1701	0.38	103.2
L3207	0.28	0.25	+0.03	91.9
L3215	0.27	0.26	+0.01	98.3
L4302	0.30	102.2
L1412	...	0.34	...	100.3
Cluster Mean Values				
$\langle \rangle$	0.33	0.32	+0.01	101.8
\pm	0.01	0.01	0.01	0.9
σ	0.05	0.05	0.05	4.6
<i>range</i>	0.25–0.40	0.26–0.41	...	91.9–114.2

^aThis study: observed photometry – predicted from modeled colors.

^bLyons *et al.* (1995) values based on measured K I column density measurements.

^c $\delta E(B-V) \equiv E(B-V)_{spec} - E(B-V)_{KI}$

^dIRAS 100 micron fluxes were obtained using IBIS, an observational planning tool for the infrared sky developed at IPAC and have been corrected for zodiacal dust contamination.

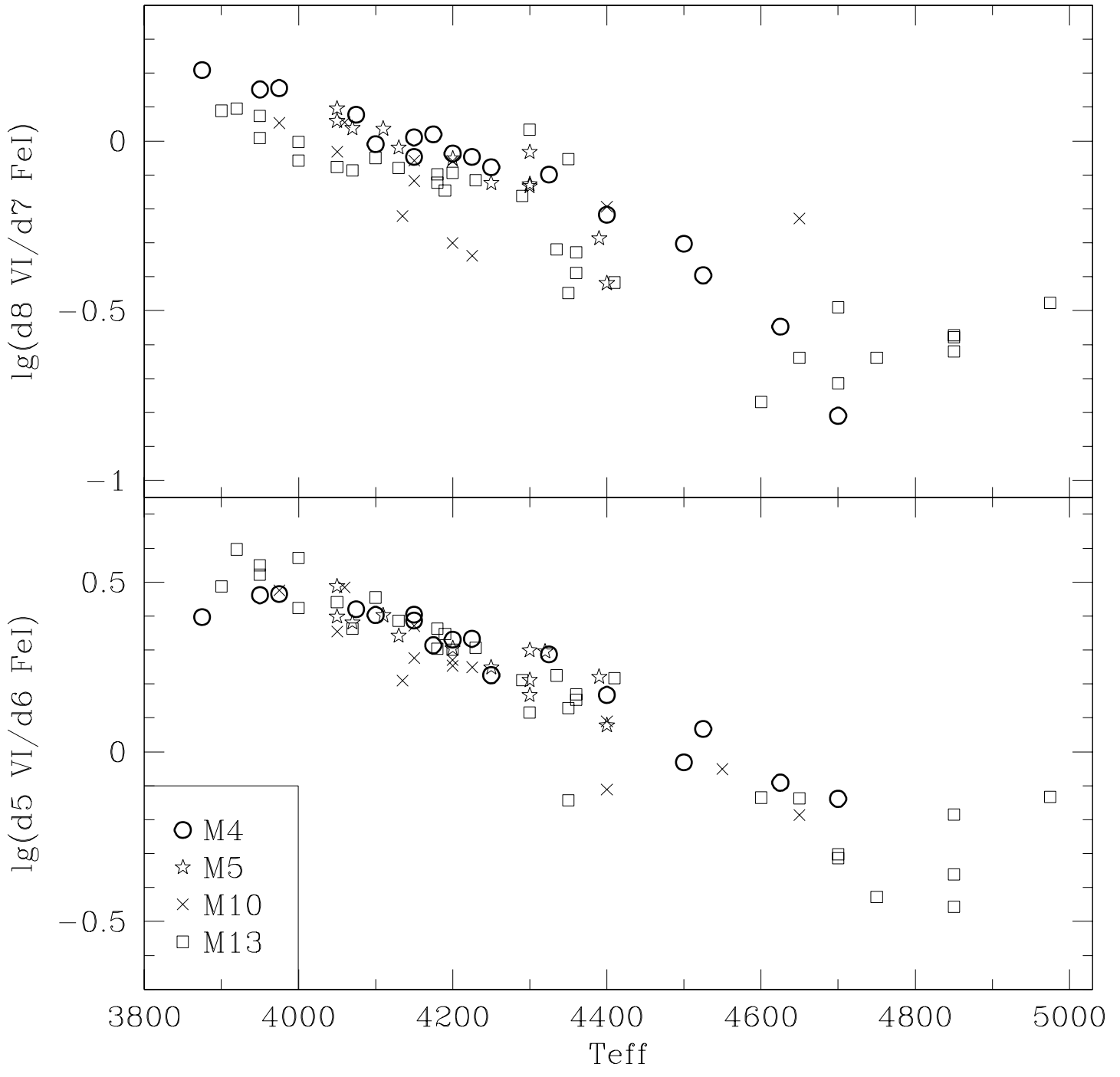


TABLE 5. Abundances in M4 Giants

Star	T_{eff}	Fe ^a	O ^b	Na	Mg	Al	Si	Ca	Sc	Ti	V	Ni	Ba	La	Eu
Abundances for Individual Stars															
L4611	3725	-1.16	+0.06	+0.33	+0.33	+0.60	+0.70	+0.04	-0.17	+0.29	-0.21	+0.11	+0.65	+0.49	+0.32
L4613	3750	-1.17	+0.05	+0.26	+0.36	+0.63	+0.52	+0.07	+0.01	+0.32	-0.11	+0.04	+0.61	+0.53	+0.34
L1514	3875	-1.16	+0.41	+0.01	+0.40	+0.44	+0.51	+0.16	-0.03	+0.29	-0.04	+0.05	+0.33	+0.42	+0.10
L1411	3950	-1.20	+0.20	+0.43	+0.47	+0.79	+0.58	+0.29	+0.03	+0.39	+0.03	+0.06	+0.68	+0.56	+0.46
L3209	3975	-1.20	+0.27	+0.23	+0.52	+0.71	+0.60	+0.35	+0.08	+0.34	+0.08	+0.04	+0.57	+0.48	+0.36
L2307	4075	-1.19	+0.17	+0.39	+0.43	+0.73	+0.54	+0.34	+0.05	+0.34	-0.05	-0.03	+0.54	+0.63	+0.42
L2406	4100	-1.20	+0.19	+0.31	+0.37	+0.55	+0.46	+0.05	-0.17	+0.25	-0.10	0.00	+0.72	+0.28	+0.25
L4511	4150	-1.18	+0.23	+0.44	+0.47	+0.83	+0.68	+0.36	+0.12	+0.37	-0.04	+0.12	+0.62	+0.56	+0.53
L1501	4150	-1.20	+0.10	+0.42	+0.42	+0.81	+0.64	+0.43	-0.03	+0.39	-0.05	+0.06	+0.62	+0.36	+0.42
L3413	4175	-1.17	+0.40	-0.04	+0.37	+0.61	+0.44	+0.28	+0.15	+0.27	-0.06	+0.05	+0.62	+0.49	+0.45
L2617	4200	-1.17	+0.01	+0.50	+0.45	+0.84	+0.61	+0.32	+0.05	+0.29	-0.05	+0.05	+0.46	+0.30	+0.33
L3624	4225	-1.16	+0.29	+0.10	+0.52	+0.69	+0.62	+0.34	+0.08	+0.33	-0.01	+0.10	+0.60	+0.49	+0.43
L3612	4250	-1.19	+0.10	+0.47	+0.48	+0.77	+0.60	+0.40	+0.07	+0.35	-0.04	+0.06	+0.64	+0.37	+0.40
L2206	4325	-1.18	+0.31	+0.25	+0.48	+0.69	+0.58	+0.36	+0.10	+0.35	-0.03	+0.08	+0.66	+0.44	+0.41
L2208	4350	-1.17	+0.36	+0.55	+0.67	+0.90	+0.60	+0.39	+0.07	+0.37	-0.04	-0.01	+0.70	+0.61	+0.55
L2519	4400	-1.16	+0.37	-0.19	+0.42	+0.50	+0.63	+0.30	-0.05	+0.25	0.00	+0.11	+0.65	+0.41	+0.40
L4201	4450	-1.18	+0.41	+0.31	+0.51	+0.55	+0.53	+0.15	+0.09	+0.19	-0.04	+0.01	+0.59	+0.33	+0.38
L4633	4500	-1.19	+0.33	-0.03	+0.35	+0.59	+0.49	+0.15	-0.15	+0.31	-0.06	+0.05	+0.60	+0.33	+0.35
L1408	4525	-1.20	+0.24	+0.18	+0.46	+0.47	+0.55	+0.27	-0.11	+0.28	-0.04	+0.04	+0.77	+0.47	+0.21
L4414	4525	-1.15	+0.16	+0.21	+0.25	+0.70	+0.43	+0.21	-0.04	+0.29	0.00	+0.07	+0.55	...	+0.22
L1701	4625	-1.20	+0.49	-0.02	+0.40	+0.62	+0.53	+0.26	-0.07	+0.25	-0.02	+0.09	+0.65	+0.44	+0.29
L3207	4700	-1.17	+0.45	-0.23	+0.36	+0.37	+0.39	+0.19	+0.01	+0.23	-0.06	+0.03	+0.66	+0.36	+0.33
L3215	4775	-1.20	+0.27	-0.03	+0.47	+0.47	+0.52	+0.25	-0.09	+0.32	-0.01	0.00	+0.39	+0.43	+0.24
L4302	4775	-1.19	+0.20	+0.31	+0.48	+0.61	+0.53	+0.16	-0.01	+0.21	+0.07	+0.05	+0.46	+0.49	+0.30
Cluster Mean Abundances															
<>		-1.18	+0.25	+0.22	+0.44	+0.64	+0.55	+0.26	+0.00	+0.30	-0.04	+0.05	+0.60	+0.45	+0.35
±		0.00	0.03	0.05	0.02	0.03	0.02	0.02	0.02	0.01	0.01	0.01	0.02	0.02	0.02
σ		0.02	0.14	0.22	0.08	0.14	0.08	0.11	0.09	0.06	0.06	0.04	0.10	0.10	0.10

^aFor this column only, metallicities [Fe/H] are given. These are the $[Fe/H]_{avg}$ values of Table 2.

^bFor this and all remaining columns, [el/Fe] values are given.

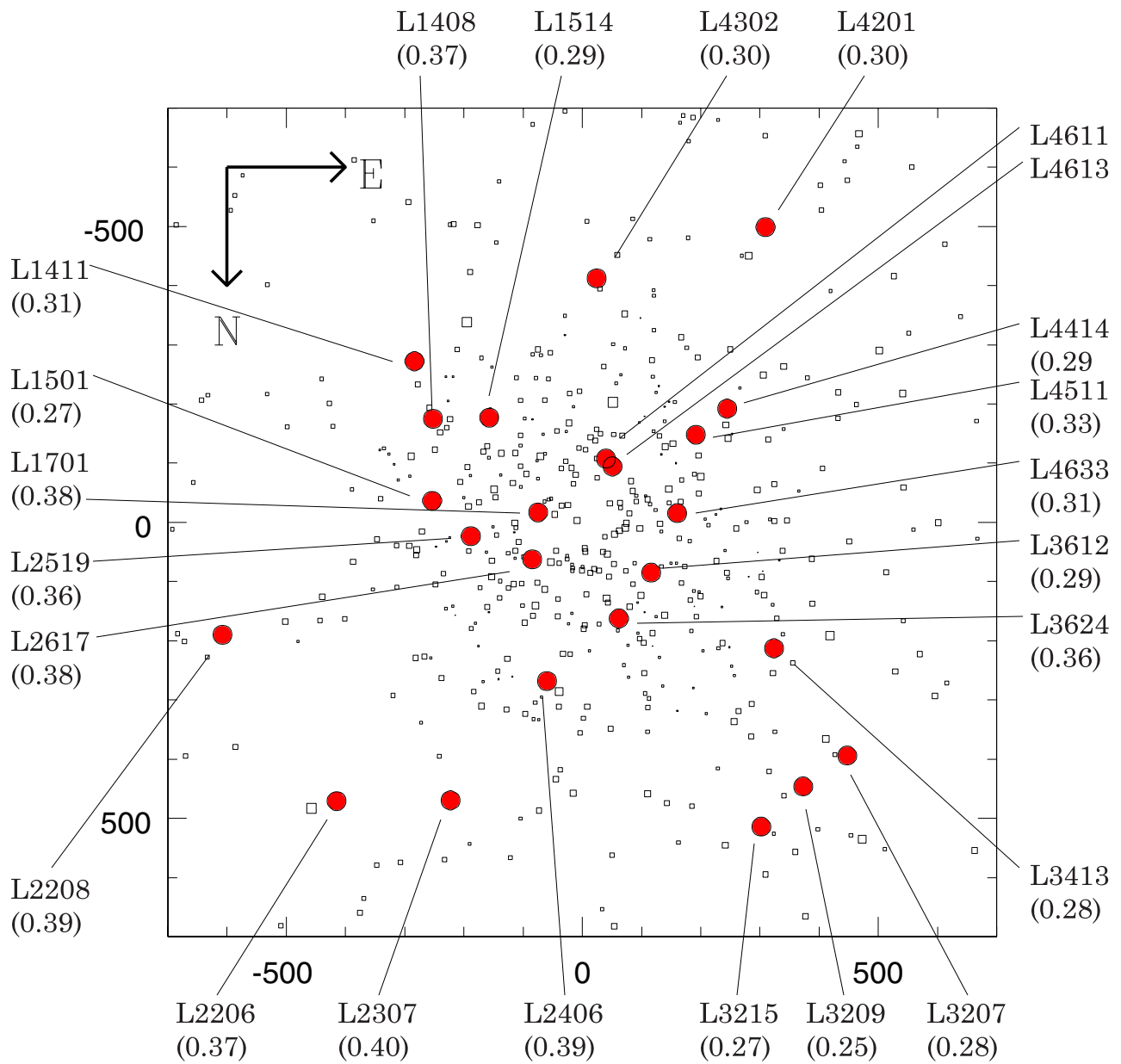


TABLE 6. Abundance Dependencies on Model Atmosphere Parameters

Quantity	δT_{eff}	δT_{eff}	$\delta \log g$	$\delta \log g$	δv_t	δv_t	δT_{eff}^a	δT_{eff}
Change =	-50 K	+50 K	-0.25	+0.25	-0.25	+0.25	-125 K	+125 K
[Fe _{avg} /H]	+0.01	-0.01	-0.08	+0.07	+0.07	-0.07	+0.04	-0.01
[Fe I/H]	-0.04	+0.04	-0.03	+0.02	+0.10	-0.10	-0.09	+0.11
[Fe II/H]	+0.06	-0.06	-0.13	+0.13	+0.04	-0.04	+0.17	-0.14
[[O I]/Fe] ^b	-0.02	+0.02	-0.02	+0.03	-0.06	+0.07	-0.06	+0.03
[Na I/Fe]	-0.06	+0.05	+0.09	-0.08	-0.06	+0.05	-0.16	+0.12
[Mg I/Fe]	-0.04	+0.04	+0.10	-0.09	0.00	0.00	-0.10	+0.09
[Al I/Fe]	-0.04	+0.04	+0.09	-0.07	-0.04	+0.05	-0.13	+0.09
[Si I/Fe]	+0.02	-0.01	+0.03	-0.01	-0.04	+0.04	+0.04	-0.03
[Ca I/Fe]	-0.07	+0.07	+0.09	-0.08	+0.02	-0.02	-0.19	+0.16
[Sc II/Fe]	0.00	0.00	-0.02	+0.03	+0.00	+0.01	+0.01	-0.01
[Ti I/Fe]	-0.10	+0.10	+0.08	-0.08	+0.01	0.00	-0.26	+0.24
[Ti II/Fe]	+0.01	-0.01	-0.03	+0.04	-0.05	+0.06	+0.01	-0.04
[V I/Fe]	-0.11	+0.12	+0.09	-0.07	-0.02	+0.04	-0.30	+0.27
[Ni I/Fe]	-0.03	+0.03	+0.03	-0.02	+0.01	0.00	-0.08	+0.08
[Ba II/Fe]	-0.02	+0.03	+0.03	-0.02	+0.07	-0.08	-0.08	+0.05
[La II/Fe]	-0.03	+0.02	-0.01	+0.01	-0.04	+0.04	-0.07	+0.04
[Eu II/Fe]	-0.01	0.00	-0.03	+0.03	-0.05	+0.05	-0.02	+0.03

^aThe first six columns illustrate the effect of random errors on individual stellar abundances; the final two columns illustrate the effect of a systematic shift on the mean abundances.

^bAll changes in [el/Fe] ratios are taken with respect to Fe_{avg}.

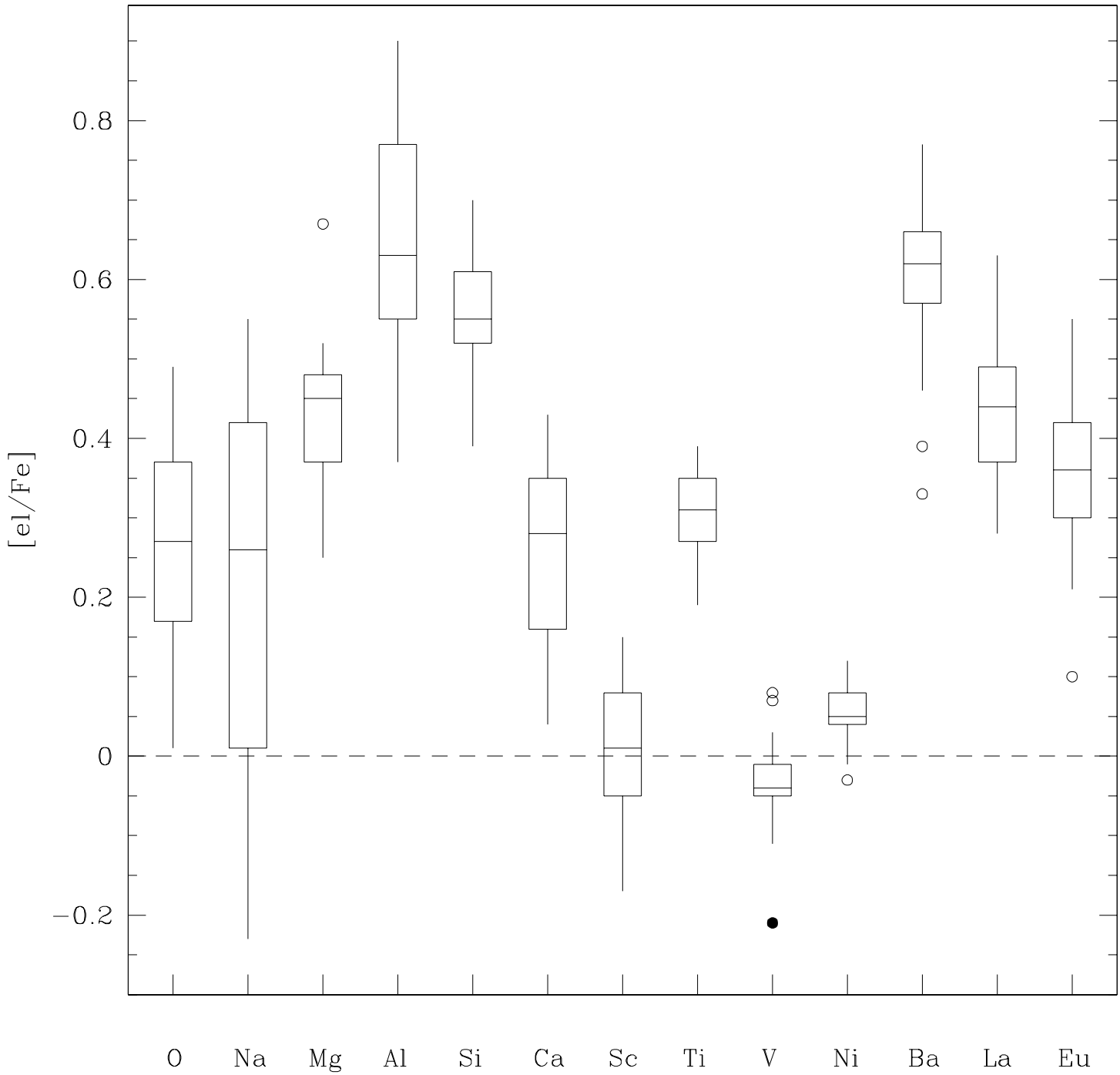


TABLE 7. Comparisons with Other M4 Work and Halo Field

Quantity	M4 this work	M4 GQO86 ^a	M4 BW92 ^b	M4 DSS92 ^c	M5 SKPL92 ^d	field ^e	M15 SKSSLP97 ^f
[Fe/H]	-1.18	-1.32	-1.21	-1.05	-1.17	...	-2.40
[O/Fe]	+0.25	...	+0.18	+0.32	+0.10	+0.31	+0.14
[Na/Fe]	+0.22	+0.31	+0.29	+0.16	-0.07	-0.17	+0.24
[Mg/Fe]	+0.44	+0.68	+0.37	...	+0.16	+0.37	+0.35
[Al/Fe]	+0.64	...	+0.80	+0.49	+0.36	-0.06	+0.79
[Si/Fe]	+0.55	+0.54	+0.51	...	+0.18	+0.30	+0.60
[Ca/Fe]	+0.26	+0.08	+0.15	+0.24	+0.19	+0.29	+0.24
[Sc/Fe]	0.00	...	+0.08	...	-0.11	+0.06	-0.13
[Ti/Fe]	+0.30	+0.24	+0.28	...	+0.29	+0.28	+0.46
[V/Fe]	-0.04	+0.13	+0.05	-0.03	-0.02
[Ni/Fe]	+0.05	-0.12	-0.10	-0.04	+0.14
[Ba/Fe]	+0.60	+0.05	+0.57	...	+0.10	-0.08	+0.10
[La/Fe]	+0.45	...	+0.45	-0.11	...
[Eu/Fe]	+0.35	...	+0.42	...	+0.45	+0.29	+0.49

^aGratton *et al.* (1986)

^bBrown & Wallerstein (1992)

^cDrake *et al.* (1992)

^dSneden *et al.* 1992 (Fe,Si,Ca,Sc,Ti,V,Ni); Shetrone 1996 (O,Mg,Al,Eu); Armosky *et al.* 1994 (Ba)

^eShetrone 1996 (O,Mg,Al); Pilachowski *et al.* 1996 (Na); Gratton & Sneden 1991 (Si,Ca,Sc,Ti,V,Ni); Gratton & Sneden 1994 (Ba,La,Eu)

^fSneden *et al.* (1997)

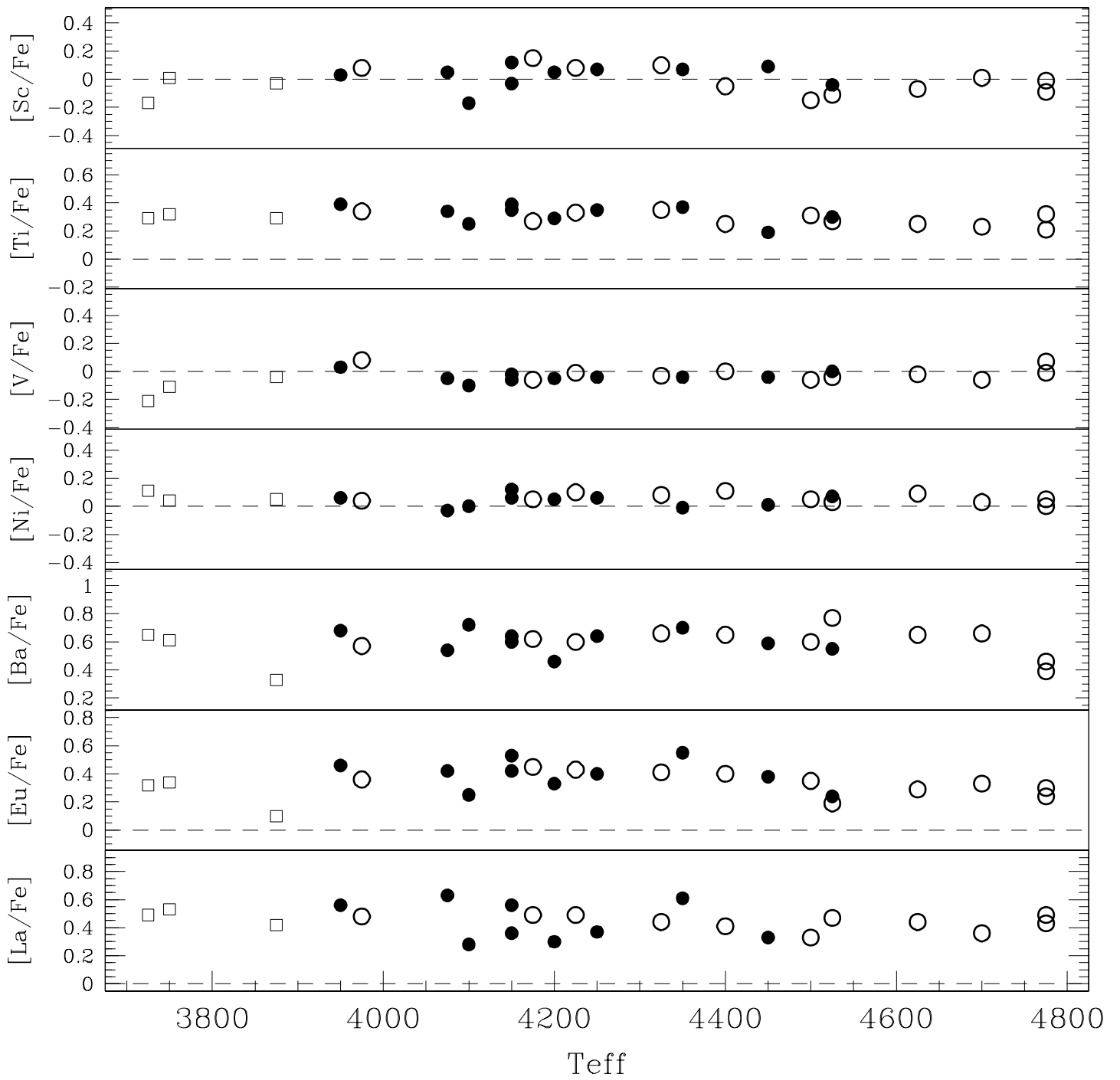


TABLE 8. CNO Abundances, Carbon Isotopic Ratios, CN Strengths

Star	T_{eff}	$\log \epsilon(\text{C})$ SS91 ^a	$\log \epsilon(\text{C})$	$\log \epsilon(\text{N})$	$\log \epsilon(\text{O})$	$\log \epsilon$ (C+N+O)	$^{12}\text{C}/^{13}\text{C}$ _b	S3839 _c	δEW7874 _d	CN?
L4611	3725	7.81	...	5.0 (3,6)	...	94	strong
L4613	3750	7.81	...	4.0 (3,6)	...	64	weak
L1514	3875	6.33	6.38	7.88	8.18	8.35	5.0 (4,6)	0.30	9	weak
L1411	3950	7.93	...	4.0 (3,7)	...	86	strong
L3209	3975	8.00	...	5.0 (3,7)	...	64	weak
L2307	4075	6.50	6.59	8.17	7.91	8.37	5.0 (4,7)	0.57	117	strong
L2406	4100	6.43	6.54	7.96	7.91	8.25	4.5 (4,6)	0.51	121	strong
L4511	4150	6.62	6.69	8.13	7.98	8.37	5.0 (4,7)	0.66	140	strong
L1501	4150	7.83	...	4.5 (3,6)	0.57	131	strong
L3413	4175	8.16	...	4.0 (3,6)	...	0	weak
L2617	4200	6.68	6.79	7.93	7.77	8.18	4.5 (4,7)	0.64	119	strong
L3624	4225	6.78	6.87	7.14	8.06	8.13	4.0 (3,5)	0.41	39	weak
L3612	4250	6.72	6.79	7.88	7.84	8.18	5.0 (4,6)	0.71	96	strong
L2206	4325	6.85	6.97	7.40	8.06	8.17	4.0 (3,5)	0.57	58	weak
L2208	4350	8.12	...	6.0 (4,8)	...	99	strong
L2519	4400	6.95	7.09	7.11	8.14	8.21	5.0 (4,7)	0.41	42	weak
L4201	4450	6.78	6.89	7.57	8.16	8.28	4.0 (3,5)	0.68	175	strong
L4633	4500	8.07	...	4.0 (3,10)	0.41	24	weak
L1408	4525	6.73	6.85	7.58	7.97	8.14	4.5 (4,6)	0.63	39	weak
L4414	4525	7.94	...	4.0 (3,5)	...	130	strong
L1701	4625	7.20	7.29	6.65	8.22	8.28	3.5 (3,6)	0.29	8	weak
L3207	4700	8.21	...	4.0 (3,7)	...	1	weak
L3215	4775	8.00	...	5.0 (3,10)	...	0	weak
L4302	4775	7.94	...	4.0 (2,7)	...	46	weak

^aThese carbon abundances are from Suntzeff & Smith (1991).

^bThe numbers in parentheses are the lowest and highest $^{12}\text{C}/^{13}\text{C}$ ratios we could deduce from our synthetic and observed spectrum matches, thus showing the uncertainties of the isotopic ratios.

^cNorris (1981), SS91, or the mean of the two sources for stars in common.

^dEW7874, T_{eff} baseline-removed.

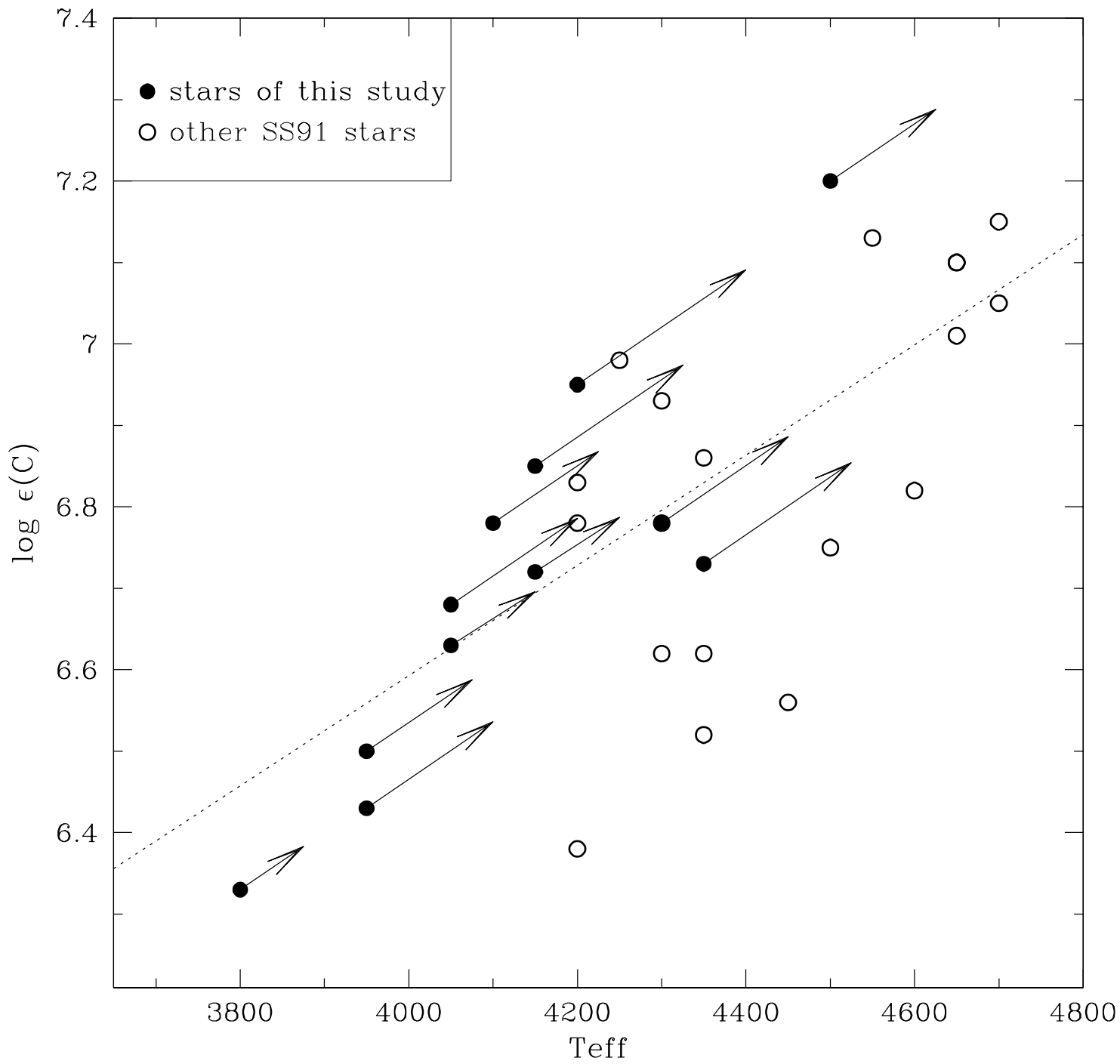


TABLE 9. Oxygen Abundances: Argus Spectra

Star	T_{eff}	[Fe/H]	[O/Fe] Argus ^a	[O/Fe] high ^b	$\delta[\text{O/Fe}]^c$
L1514	3875	-1.20	+0.41	+0.41	0.00
L1411	3950	-1.20	+0.07	+0.20	-0.13
L3209	3975	-1.20	+0.22	+0.27	-0.05
L4511	4150	-1.18	+0.22	+0.23	-0.01
L3413	4175	-1.17	+0.32	+0.40	-0.08
L2617	4200	-1.17	+0.07	+0.01	+0.06
L3624	4225	-1.16	+0.27	+0.29	-0.02
L3612	4250	-1.19	+0.12	+0.10	+0.02
L1403	4323	-1.18	+0.22
L2206	4325	-1.18	+0.22	+0.31	-0.09
L2608	4366	-1.18	+0.37
L2519	4400	-1.16	+0.37	+0.37	0.00
L4413	4427	-1.18	+0.27
L2305	4430	-1.18	+0.22
L4201	4450	-1.18	+0.42	+0.41	+0.01
L4415	4505	-1.18	+0.37
L4421	4521	-1.18	+0.07
L1408	4525	-1.20	+0.22	+0.24	-0.02
G273	4532	-1.18	+0.52
L4105	4535	-1.18	-0.08
L2410	4548	-1.18	+0.32
L4206	4593	-1.18	+0.52
L1617	4609	-1.18	+0.17
L1701	4625	-1.20	+0.52	+0.49	+0.03

^a[O/Fe] values from the Argus medium resolution spectra.

^b[O/Fe] values from the McDonald and Lick high resolution spectra.

^c $\delta[\text{O/Fe}] \equiv [\text{O/Fe}]_{\text{Argus}} - [\text{O/Fe}]_{\text{high}}$.

